

University of Windsor

## Scholarship at UWindor

---

Electronic Theses and Dissertations

Theses, Dissertations, and Major Papers

---

1996

### Ripple morphology in a sand/mud environment: Guyana, South America.

Jr. Curkovic, Josip  
*University of Windsor*

Follow this and additional works at: <https://scholar.uwindsor.ca/etd>

---

#### Recommended Citation

Curkovic, Josip, Jr., "Ripple morphology in a sand/mud environment: Guyana, South America." (1996).  
*Electronic Theses and Dissertations*. 3352.  
<https://scholar.uwindsor.ca/etd/3352>

This online database contains the full-text of PhD dissertations and Masters' theses of University of Windsor students from 1954 forward. These documents are made available for personal study and research purposes only, in accordance with the Canadian Copyright Act and the Creative Commons license—CC BY-NC-ND (Attribution, Non-Commercial, No Derivative Works). Under this license, works must always be attributed to the copyright holder (original author), cannot be used for any commercial purposes, and may not be altered. Any other use would require the permission of the copyright holder. Students may inquire about withdrawing their dissertation and/or thesis from this database. For additional inquiries, please contact the repository administrator via email ([scholarship@uwindsor.ca](mailto:scholarship@uwindsor.ca)) or by telephone at 519-253-3000ext. 3208.

## INFORMATION TO USERS

This manuscript has been reproduced from the microfilm master. UMI films the text directly from the original or copy submitted. Thus, some thesis and dissertation copies are in typewriter face, while others may be from any type of computer printer.

**The quality of this reproduction is dependent upon the quality of the copy submitted.** Broken or indistinct print, colored or poor quality illustrations and photographs, print bleedthrough, substandard margins, and improper alignment can adversely affect reproduction.

In the unlikely event that the author did not send UMI a complete manuscript and there are missing pages, these will be noted. Also, if unauthorized copyright material had to be removed, a note will indicate the deletion.

Oversize materials (e.g., maps, drawings, charts) are reproduced by sectioning the original, beginning at the upper left-hand corner and continuing from left to right in equal sections with small overlaps. Each original is also photographed in one exposure and is included in reduced form at the back of the book.

Photographs included in the original manuscript have been reproduced xerographically in this copy. Higher quality 6" x 9" black and white photographic prints are available for any photographs or illustrations appearing in this copy for an additional charge. Contact UMI directly to order.

# UMI

A Bell & Howell Information Company  
300 North Zeeb Road, Ann Arbor MI 48106-1346 USA  
313/761-4700 800/521-0600



**RIPPLE MORPHOLOGY IN A SAND/MUD ENVIRONMENT:  
GUYANA, SOUTH AMERICA**

by  
Josip Curkovic Jr.

A Thesis Submitted  
to the Faculty of Graduate Studies and Research  
through the Department of Geography  
in Partial Fulfillment of the Requirements for  
the Degree of Master of Arts at the  
University of Windsor

Windsor, Ontario, Canada

1996

© 1996 Josip Curkovic Jr.



National Library  
of Canada

Acquisitions and  
Bibliographic Services

395 Wellington Street  
Ottawa ON K1A 0N4  
Canada

Bibliothèque nationale  
du Canada

Acquisitions et  
services bibliographiques

395, rue Wellington  
Ottawa ON K1A 0N4  
Canada

*Your file Votre référence*

*Our file Notre référence*

The author has granted a non-exclusive licence allowing the National Library of Canada to reproduce, loan, distribute or sell copies of this thesis in microform, paper or electronic formats.

The author retains ownership of the copyright in this thesis. Neither the thesis nor substantial extracts from it may be printed or otherwise reproduced without the author's permission.

L'auteur a accordé une licence non exclusive permettant à la Bibliothèque nationale du Canada de reproduire, prêter, distribuer ou vendre des copies de cette thèse sous la forme de microfiche/film, de reproduction sur papier ou sur format électronique.

L'auteur conserve la propriété du droit d'auteur qui protège cette thèse. Ni la thèse ni des extraits substantiels de celle-ci ne doivent être imprimés ou autrement reproduits sans son autorisation.

0-612-30897-9

## ABSTRACT

Ripples formed under oscillatory flows in a field setting are examined to construct a simple and accurate method of predicting ripple wavelength in a sand/mud environment. The variables that determine ripple wavelength are very complex, and at least four nondimensional parameters are important. For practical purposes the ripple wavelength normalized by the water semi-excursion (half the orbital diameter) is well determined by the mobility number and the normalized orbital diameter. Ripples with wavelengths proportional to grain size and independent of orbital diameter (anorbital ripples) were predominant in this investigation (60%). Wavelengths dependent on both orbital diameter and grain size (suborbital ripples) constituted the remaining ripples observed. Relating normalized ripple wavelength to the mobility number shows a strong correlation ( $r^2=0.7049$ ). However, the normalized ripple wavelength is best explained by the normalized orbital diameter ( $r^2=0.7936$ ). Equations derived by other workers to predict ripple wavelength in quartz sand were only moderately successful with fine grain sediments. Therefore, a set of expressions were developed based on the mobility number and the orbital diameter. The derived semi-empirical formulae provide a more accurate method of predicting ripple wavelength for a large set of data from a sand/mud environment.

## ACKNOWLEDGEMENTS

I am very grateful to Dr. A.S. Trenhaile, Dr. V.C. Lakhan and Dr. P.D. LaValle for their insight in the field of ripple morphology making this investigation possible. Without Dr. I.S. Al-Aasm's suggestions, the sediment data analysis would not have been feasible. Appreciation goes out to Trent University, Department of Geography, especially to Dr. C. McKenna-Neuman for the use of their Particle Size Analysis Laboratory. I would also like to acknowledge Mr. Dave Webster and Mr. Ron Welch, and the entire Geography Department for their assistance throughout this project. The author is indebted to my many friends at the University of Windsor, especially Lloyd M. Prevedel, Bernie Rourke, and Mikael Dalimonte, without their suggestions and support this investigation would not come to fruition. Many thanks also to the many people in Guyana, including Mr. and Mrs. Navin Chandarpal, Mohan Mangal, Mohandat "Rico" Goolsaran, Mangal Chandraka, Philip Kartick, and Zakin Yamin. Finally, thanks goes to TLK for being so understanding.

## TABLE OF CONTENTS

Abstract . . . . .	iii
Acknowledgements . . . . .	iv
List of Figures . . . . .	vi
List of Tables . . . . .	vi
List of Abbreviations . . . . .	vii

### CHAPTER

1.0 INTRODUCTION . . . . .	1
2.0 REGION UNDER STUDY . . . . .	5
2.1 Mineralogy of Beach Sediment . . . . .	10
3.0 REVIEW OF THE LITERATURE . . . . .	13
3.1 Ripple Morphology . . . . .	13
3.2 Ripple Train . . . . .	14
3.3 Environmental Distribution of Ripples . . . . .	17
3.4 Geological Significance . . . . .	17
3.4 Empirical Relationships . . . . .	19
4.0 CONCEPTUAL BASIS OF THE STUDY . . . . .	25
4.1 Hypotheses . . . . .	27
5.0 METHODOLOGY . . . . .	29
6.0 BEDFORM TYPES . . . . .	36
Type I: Straight Ripple-trains . . . . .	36
Type II: Sinuous Ripple-trains . . . . .	38
Type III: Linguoid Ripple-trains . . . . .	38
Type IV: Catenary Ripple-trains . . . . .	39
7.0 RESULTS AND DISCUSSION . . . . .	40
7.1 Assessment of Hypothesis #1 . . . . .	40
7.2 Assessment of Hypothesis #2 . . . . .	51
7.3 Suggestions for Further Study . . . . .	55
8.0 CONCLUSIONS . . . . .	57
REFERENCES . . . . .	60
APPENDIX I . . . . .	64
APPENDIX II . . . . .	67
VITA AUCTORIS . . . . .	79



## LIST OF FIGURES

### FIGURE

1.	Growth of Vortices over a Rippled Bed	3
2.	The Natural Regions of Guyana	6
3.	The Study Area	7
4a.	Beach Topography	8
4b.	The Nearshore Cell Circulation Patterns at High Tide	9
4c.	The Nearshore Cell Circulation Patterns at Low Tide	9
5.	Characteristics of Smallscale Ripples	15
6.	Idealized Ripple Trains	16
7.	A Priori Model	26
8.	Sampling Stations	30
9.	Ripple Marks in Profile	31
10.	Straight Transverse Ripples	36
11.	Swept Ripples	37
12.	Transverse Sinuous Ripples in Phase	38
13.	Transverse Sinuous Ripples out of Phase	38
14.	Linguoid Ripples	39
15.	Catenary Ripples	39
16.	Classification of Ripples based on the Relationship Between $\lambda/D$ as a function of $d_o/D$	44
17.	$\lambda/D$ as a function of $d_o/D$	45
18.	$\lambda/a$ as a function of $d_o/D$	48
19.	Comparison of the predicted relationships for $\lambda/a$ as a function of $d_o/D$	49
20.	$\lambda/a_{\text{predicted}}$ versus $\lambda/a_{\text{measured}}$ (using equation 7)	50
21.	$\lambda/a$ as a function of the mobility number	52
22.	$\lambda/a_{\text{predicted}}$ versus $\lambda/a_{\text{measured}}$ (Nielsen, 1981)	53
23.	$\lambda/a_{\text{predicted}}$ versus $\lambda/a_{\text{measured}}$ (using equation 8)	53

## LIST OF TABLES

### TABLE

1.	Ripple and Wave Data	41
----	----------------------	----

## LIST OF ABBREVIATIONS

$u_m$	-maximum bottom orbital diameter	$h$	-water depth
$\Delta u_m$	-velocity asymmetry	$L$	-wave length
$D$	-median grain size	$\psi$	-mobility number
$T$	-wave period	$a$	-water semi excursion (half the orbital diameter)
$\lambda$	-ripple wavelength	$2\pi/T$	-wave radian frequency
$d_o$	-orbital diameter	$s$	-relative sediment density
$H$	-wave height	$g$	-acceleration of gravity

# **RIPPLE MORPHOLOGY IN A SAND/MUD ENVIRONMENT: GUYANA, SOUTH AMERICA**

## **CHAPTER 1.0**

### **INTRODUCTION**

Nearshore ripple marks, which are produced by wind-generated waves and currents, begin to develop with the initial movement of sediment. Small-scale ripples are generally less than 4 cm in height and 60 cm in length, and they are arranged transversely to flow (Allen, 1968; Boyd *et al.*, 1988). Ripple profiles are controlled by the nature of near-bottom wave motion, current strength and direction, and the size of the bed material (Dingler and Inman, 1976). The sub-ripple bed may consist of loose grains, cohesive mud, or rock.

Bagnold (1946) distinguished two types of oscillation ripples. The ripples that first arise on a level bed affected by progressive waves are only a few grains in height, with rounded crests and, in fine sands, nearly plane troughs. These *rolling grain* ripples become stable when the troughs are completely sheltered and the crests are unable to accumulate any more grains. Some workers believe that rolling grain ripples are stable, while others suggest that they represent only a transient stage in the development of vortex ripples. *Vortex ripples*, which generally have a steep leeside and a gently sloping stoss-side, tend to develop when there are low to moderate rates of sediment transport. Any perturbation on a flat bed can cause flow separation, whereby the zone of high shear leaves the bed and rejoins it a short distance

downstream. Vortices, which develop to the leeside of ripples every half wave cycle, propel grains towards the ripple crests until the flow reverses. At the end of the return stroke, a second vortex develops on the other side of the ripple, and this too lifts sediment into the flow (Fig. 1). The present paper is concerned only with small-scale vortex ripples.

The formation and morphology of bedforms is of considerable interest because they exert an important influence over sediment transport, wave attenuation, and wave induced currents. Hydraulic engineers, for example, have long studied the movement of sediment over bedforms in order to better understand flooding patterns, and to plan of navigation and irrigation strategies. In addition, geologists study ripples as sedimentological features in sedimentary rocks in the belief that they are to some extent diagnostic of the sedimentary and hydrodynamic environment.

Numerous studies have investigated the relationship between wave parameters, grain size and ripple geometry in laboratory and field settings. Laboratory studies include those of Bagnold (1946), Manohar (1955), Yalin and Russell (1962), Kennedy and Falcon (1965), Horikawa and Watanabe (1967), Carstens *et al.*, (1969), Mogridge and Kamphuis (1972), Trenhaile (1973), Sleath (1975), Clifton (1976), Allen (1979), Miller and Komar (1980a), Nielsen (1981), Vongvisessomjai (1984), Kos'yan and Kochergin (1992), Ranasoma and Sleath (1992), and Mogridge *et al.* (1994). One major constraint of these investigations is the short, monochromatic waves used in most cases because of the limitations of the laboratory apparatus. Field investigations include those of Inman (1957), Dingler and Inman (1976), Allen (1979), Miller and

## GROWTH OF VORTICES OVER A RIPPLED BED

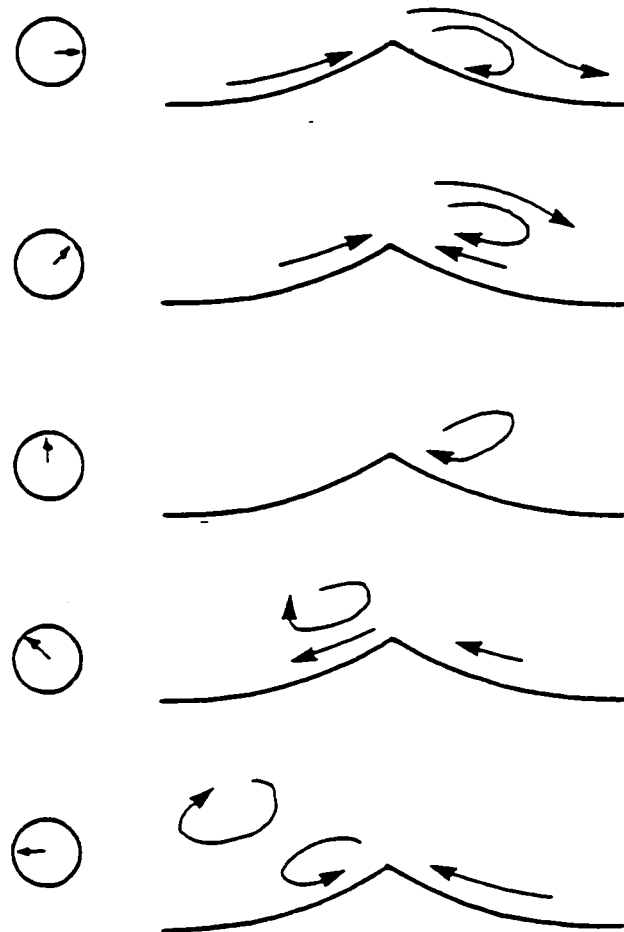


**Figure 1:** The sequence of events during a wave oscillation showing the formation separation and advection of vortices. The vectors along the left side indicate the direction of flow (Dyer, 1986).

Komar (1980b), Grant and Madsen (1982), Vongvisessomjai (1984), Boyd *et al.* (1988), Kawata *et al.* (1992), Kos'yan and Kochergin (1992), Osborne and Vincent (1993), Mogridge *et al.* (1994), and Wilberg and Harris (1994). Average wave period is generally longer in field investigations than in laboratory studies, but the wave field is typically comprised by a range of wave heights and periods, complicating interpretation of the relationship between wave conditions and measured ripple geometry. Although the importance of bedforms is well documented, it is only recently that we are starting to understand the conditions under which they develop, the factors that determine their geometry, and the energy contained in the vortices that form above them (Trenhaile, in press). The purpose of the present paper was to examine small-scale vortex ripple wavelength across the nearshore zone of a sand/mud environment, and, on the basis of the field data, to determine the relationships that exist between ripple wavelength, orbital diameter, and mean grain size.

## CHAPTER 2.0

### REGION UNDER STUDY

Guyana is located above the equator on the northern coast of South America between 0°41' N and 8°33' N and between 56°32' W and 61°22' W. It is bounded by the Atlantic Ocean to the north, Brazil to the south, Surinam to the east, and Venezuela to the west (Fig. 2). Most of the 2000-2500 mm/year of rainfall occurs during two peak periods, May-June and December-January. Winds are consistently between northeast and north-northeast. The coast is meso-to-microtidal, with a mean spring tidal range of 2.38 m and a neap range of 1.9 m. The coastal plain is occupied by mangroves near the coastline, interdispersed with a network of chenier ridges and migratory mudflats. These mudflats not only influence the hydrodynamic and climatic processes but they also have an important impact on coastal evolution (Froidefond *et al.*, 1988). Two predominant sources contribute to the high concentration of suspended sediment in the nearshore zone (Allersma, 1968): sediment from local rivers (for example, the Corentyne, Berbice, Demerara, Essequibo, Mahaica, and Mahaicony); and material carried north-westwards by longshore currents from the Amazon Basin.

Field measurements of ripple spacing and wave parameters were obtained off Melanie Beach, which is located within the District of Bachelor's Adventure, approximately 16 kilometres east of the capital, Georgetown (Fig. 3). The beach is subject to high wave energy conditions with a well defined set of swell waves present.

# The Natural Regions of Guyana

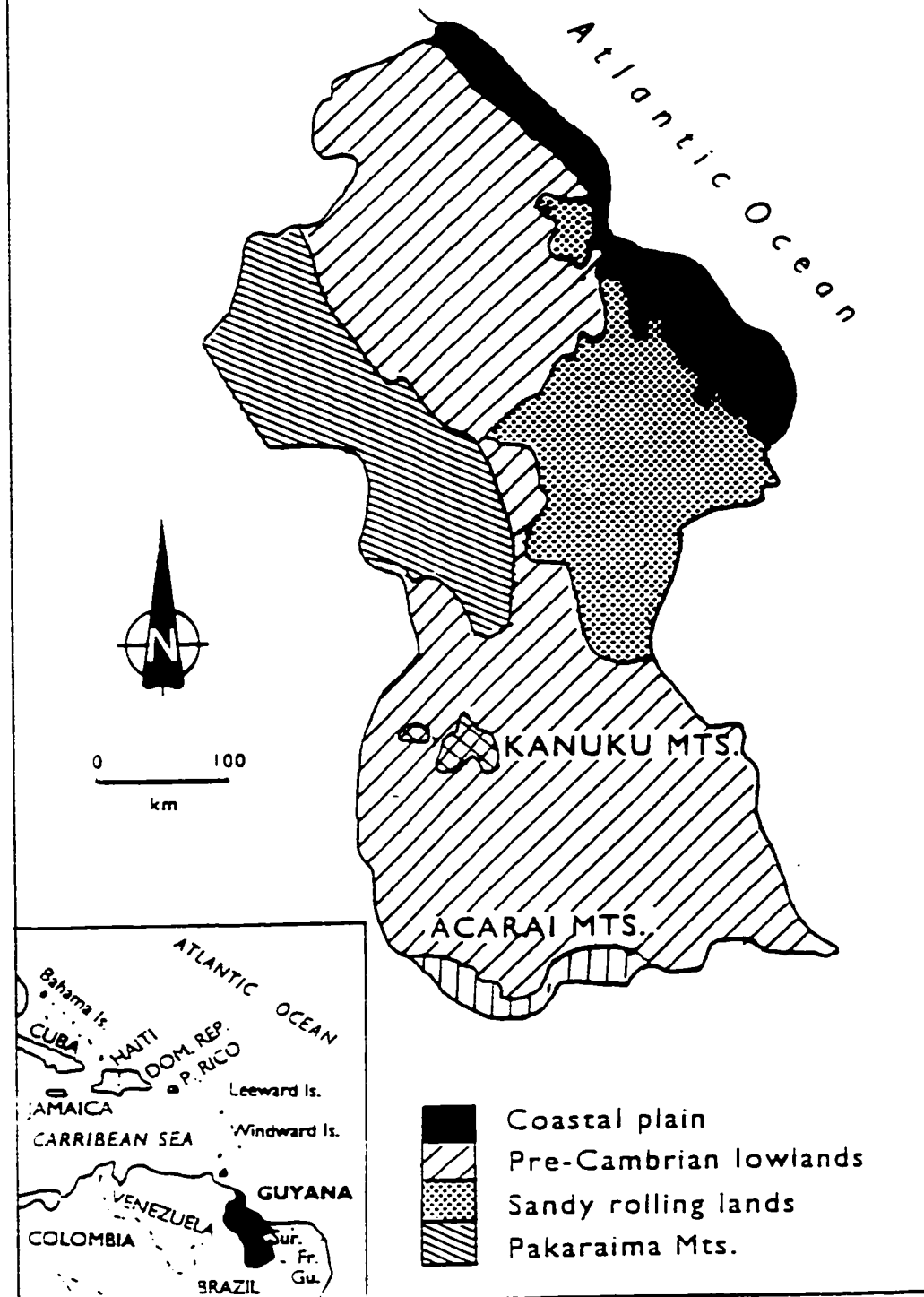


**Figure 2**

(Source: Lakhan, 1994)



## THE STUDY AREA

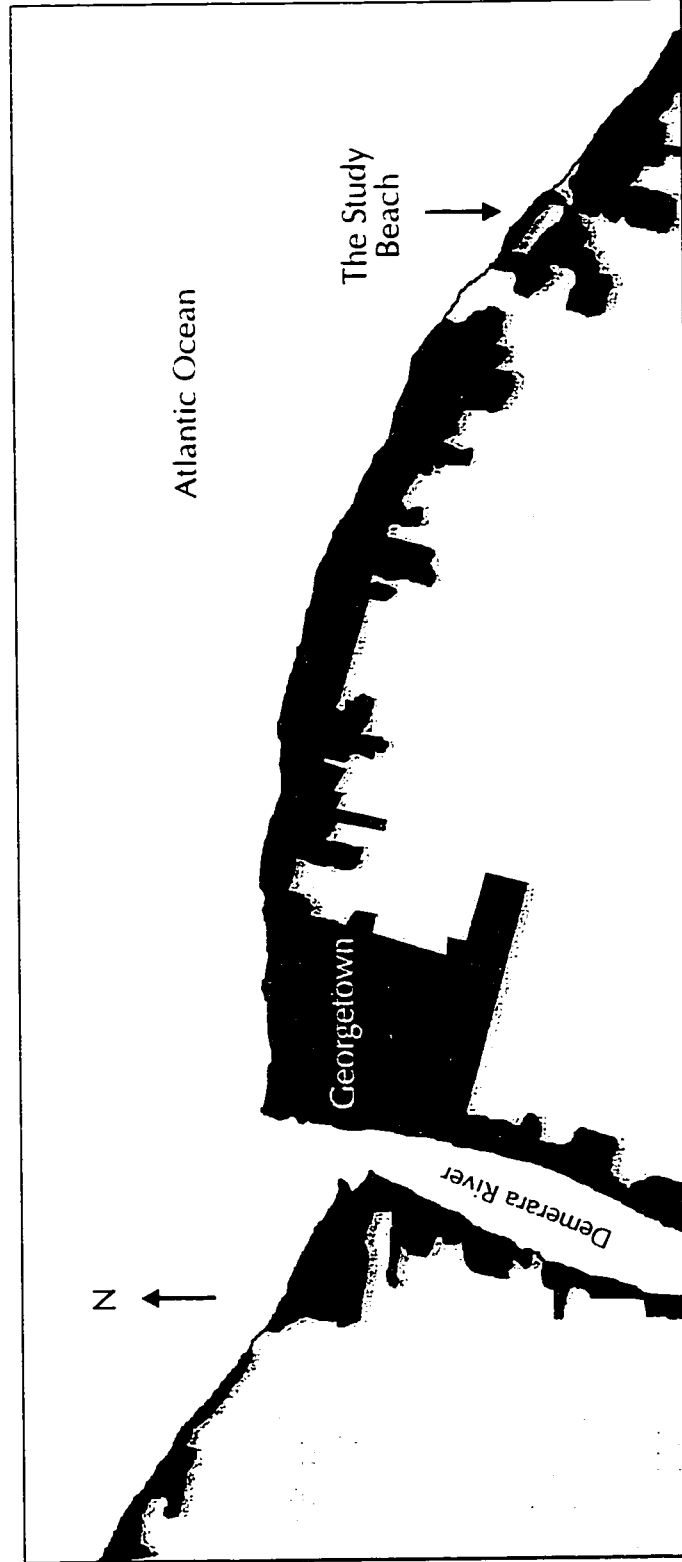


Figure 3

Scale: 1:157 204

### LEGEND

	Cultivated Land		Beach Area
	City or Built Up Area		Ocean

Source: Author, 1996

# BEACH TOPOGRAPHY

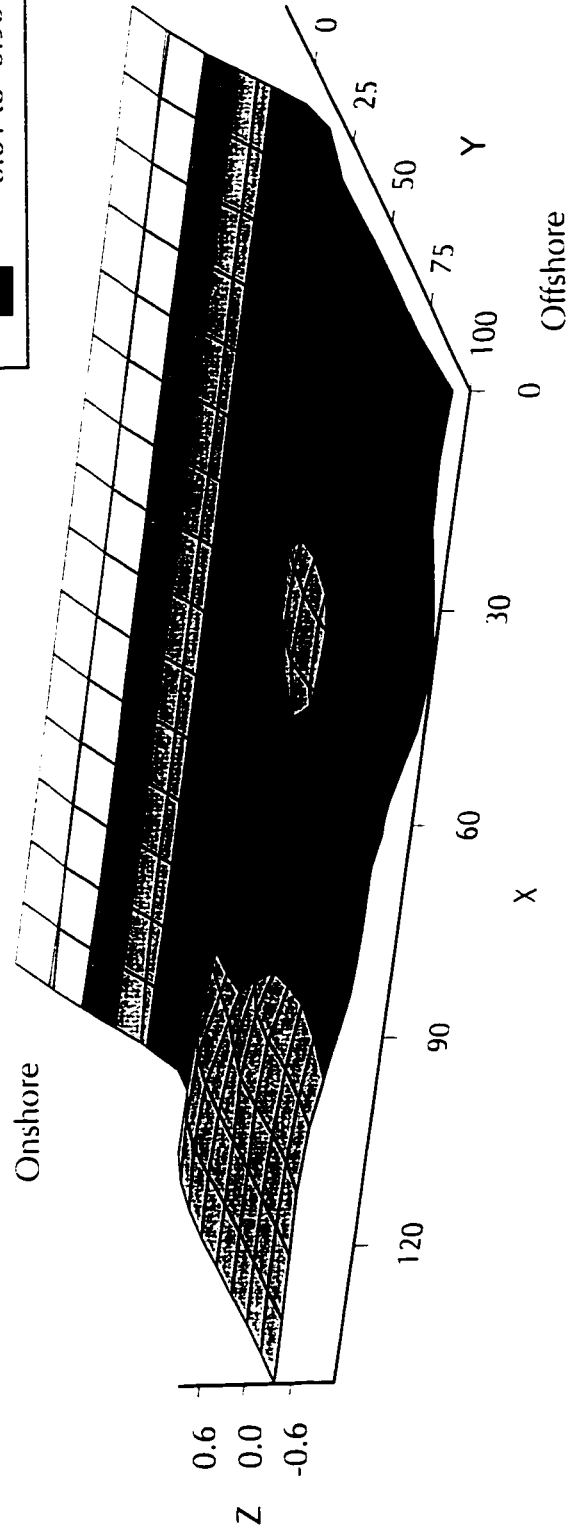
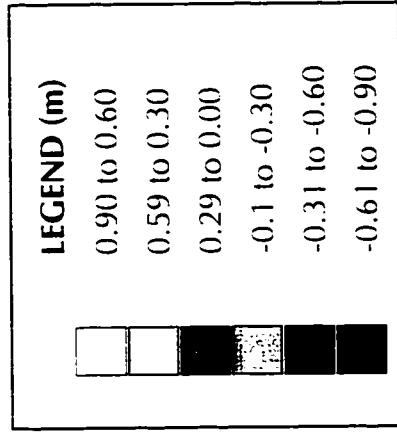


**Figure 4a**

Source: Author, 1996

Note: All values are in meters.

## The Nearshore Cell Circulation Patterns at High Tide

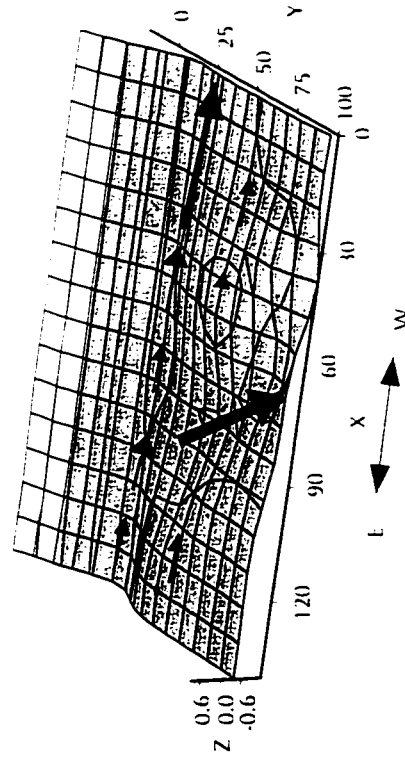


**Figure 4b:** The summation of cell circulation and a longshore current from oblique waves resulting in an observed rip current in the nearshore. Rip currents carved a shallow, narrow channel through the nearshore bar that ran seawards from the trough to the northwest.

Note: Grey areas indicate water.

## The Nearshore Cell Circulation Patterns at Low Tide

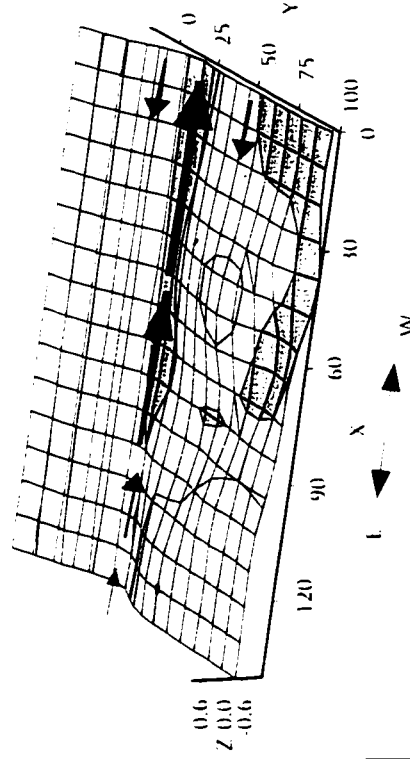


**Figure 4c:** During low tide the channel was subject to gravity driven ebb flow drainage, although a wave occasionally travelled back up the trough to the east. This wave was probably generated by large infragravity wave groups at the end of the bar to the west.

Note: Grey areas indicate water.

Note: All values are in meters.

The investigation was conducted within a surf zone that extended up to 80 metres seaward from the beach, in water depths ranging from 0.2 to 0.8 metres. The upper shore consists of a shell chenier ridge abutting a seawall constructed to protect Guyana's low lying coastal plain. The overall beach slope is gentle (between 1 and 3 degrees), although its topography is irregular, consisting of a deep narrow trough running parallel to the shore and lying landward of a large, gentle sloping bar with its crest approximately at the midsurf position (Fig. 4a). During field observations in June-July of 1994, the nearshore was influenced by incident waves with periods of between 5 and 8 seconds and wave heights of between 0.2 and 0.6 metres. Angles of wave approach were consistently between 331 and 347 degrees. Nearshore currents were generated by integrated longshore and cell circulation rip current systems (Fig. 4b,c).

## **2.1 Mineralogy of Beach Sediment**

The bottom sediment in the study area is poorly sorted and grain size distribution were bimodal. Mean grain size ranged from  $55.8\mu\text{m}$  to  $103.6\mu\text{m}$  and standard deviation from  $42.6\mu\text{m}$  to  $82.3\mu\text{m}$ . The relative sediment density is  $2.65\text{ g/m}^3$  and coarse silt and very fine sand are the dominant component. Other constituents included heavy minerals in the fine fractions, and abundant shell fragments of coarse-sand size.

The lighter fractions of heavy minerals generally consist of a very limited number of constituents; feldspar, mica, and volcanic glass are the principal ones

(Nota, 1958). The principal components of the heavy mineral assemblages off the Guyana coast include; tourmaline, zircon, staurolite, andalusite, sillimanite, epidote, hornblende, and hypersthene. Of the heavy minerals, four mineral associations can be distinguished (Nota, 1958).

The *Epidote-Hornblende* (EH) association is the dominant type of sediment for the area off the Orinoco river. Other than epidote and hornblende, zircon occurs in significant amounts. The minerals of the metamorphic group (staurolite, andalusite and sillimanite) make up the minor components. The *Staurolite* (ST) association contains high percentages of metamorphic minerals, and its most significant feature is the relatively high content of staurolite. The distribution pattern of the ST sands extends offshore in a zone parallel to the coast between the Orinoco and Essequibo rivers. The most notable characteristic of the third mineralogical province, the *Epidote-Hornblende-Hypersthene* (EHH) association, is the presence of hypersthene in notable amounts. Its distribution area is relatively small, located directly off the mouth off the Essequibo river.

The mineralogical province in which this investigation was carried out may be classified mineralogically as an *Epidote-Hornblende* deposit, with varying amounts of *Metamorphic* minerals (EHM). The EHM mineral province extends off the Demerara river and approximately 50 kilometres eastward. Unlike the ST sands, the EHM sediments have relatively low amounts of staurolite, and they differ from the EH deposits in their higher content of metamorphic minerals and comparatively smaller amount of hornblende. The very fine-grained sediments of this mineral province

contain a good deal of zircon, with the dominant metamorphic mineral in this association being sillimanite.

## CHAPTER 3.0

### REVIEW OF THE LITERATURE

Workers from various disciplines have tried to determine the reasons for ripple formation and the relationship between their morphology, grain size, and wave conditions. Some approaches have been theoretical and have suggested that the causative agents related to turbulence in the fluid. Other studies have been empirical and have sought to define, largely from experimental or from field observations, the ranges of wave parameters under which ripples develop.

#### 3.1 Ripple Morphology

One of the most interesting features of ripples is their uniformity of size and spacing under any one set of conditions. Long-crested ripples, for example, are elongated transversely to flow and are quasi-regularly spaced. Ripples of this kind may be called *transverse*. In contrast, parting lineations are elongated parallel to the flow and occur at regular intervals transversely across the flow. The term *longitudinal* is applicable to ripples of this type (Allen, 1968).

The anatomy of ripples can be treated as having three-dimensional or two-dimensional geometry (Allen, 1968). Three-dimensional ripples vary substantially in height along the span, and the crestline is locally skewed to the flow at a angle significantly different from 90°. All ripples have in reality a three-dimensional geometry, for their dimensions of height, length and width are finite. From the

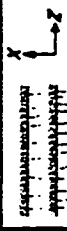
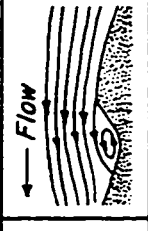



standpoint of fluid flow, however, some kinds of ripples can be treated as two-dimensional when only two coordinates need to be referred to. Ripples of this type have a length which is large compared to their height. Two-dimensional ripples are therefore fairly uniform in height along the span and have essentially straight crests at right angles to the flow. When height, width and length are all of the same order, however, the ripple must be treated as three-dimensional. As noted earlier, this thesis is only concerned with small-scale vortex ripples. These ripples assume several different forms (Fig. 5). Some have long straight crests while others, although long-crested, are somewhat sinuous in plan. Many ripples are distinguished by short, markedly curved crestlines which close down-current.

### 3.2 Ripple Train

The term *ripple-train* refers to an areal unit within the bounds of which occur ripple marks of similar shape, scale and orientation (Allen, 1968). Therefore, ripple trains are generally, made up of a large number of similar ripples (Fig. 6). There is, of course, only one mutual arrangement that can be adopted by straight crested ripples (Fig. 6a). Sinuous and catenary ripples, on the other hand, are arranged in two distinct ways. When the crests and troughs are parallel to the flow, the ripples are said to be *in phase* (Fig. 6c, e), and when crests alternate with troughs parallel to flow, the ripples are *out of phase* (Fig. 6d, f). It is not uncommon to find straight and catenary ripple trains whose individual ripples are sharply skewed relative to the general flow. Such ripple trains are termed *swept* (Fig. 6b, g). The most common mode of



## Characteristics of Small Scale Ripples

BED FORM	SHAPE	PHYSICAL SCALE (in grain diameters)	GEOMETRY	RELATION TO MAIN COMPONENT OF FLOW	FLOW PATTERN	INSTABILITY PATTERN
Smallscale ripples		Height $\approx 2 \times 10^1 D$	Two-dimensional	Transverse		Longitudinal
			Three-dimensional			
				Transverse with longitudinal elements		

**Figure 5:** The X coordinate is parallel to flow, and the Z coordinate perpendicular to flow. (Source: Allen, 1969)

# Idealised Ripple Trains

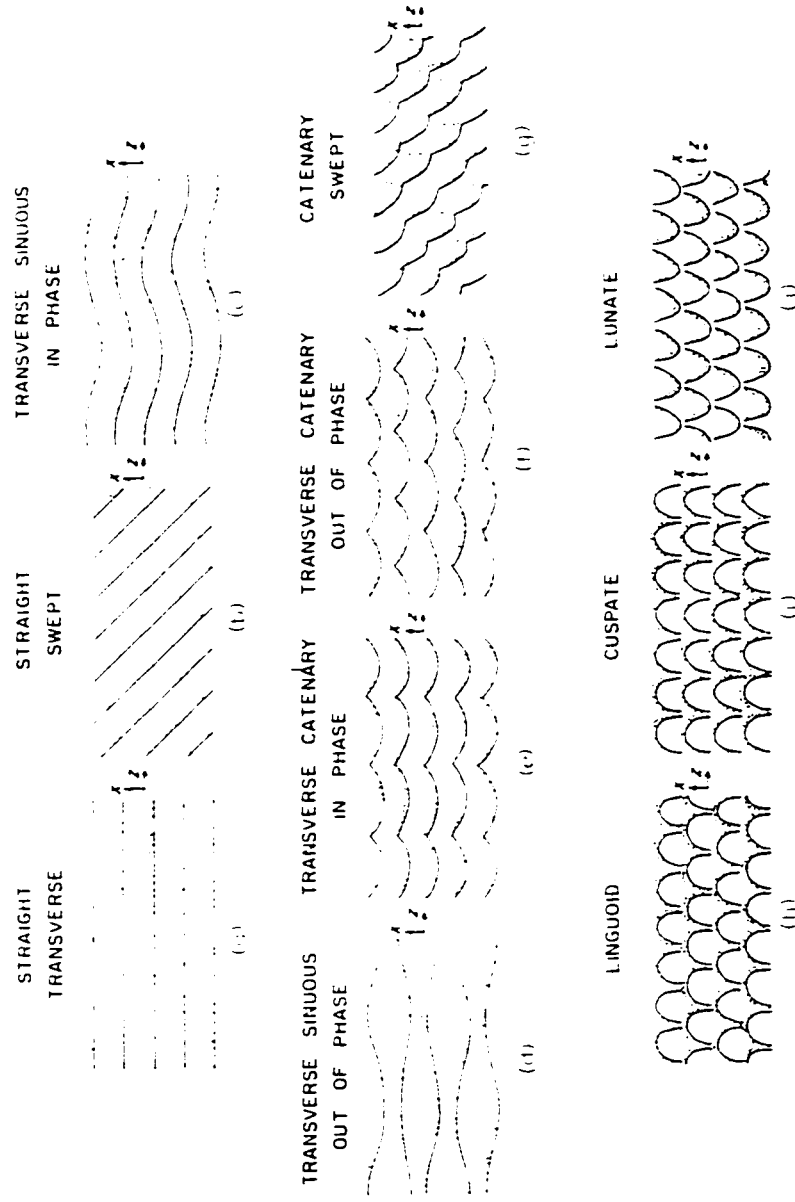


**Figure 6:** The X coordinate is parallel to flow, and the Z coordinate perpendicular to flow. Leesides and spurs are stippled. (Source: Allen, 1969)

arrangement of linguoid ripples, and the only known arrangement of lunate ripples, is an offset relationship between the ripples of successive rows, the ripples therefore being out of phase (Fig. 6h, j). These ripple trains show strong diagonal as well as transverse patterns. Very rarely linguoid ripples can have an in phase arrangement. These ripple trains are referred to as *cusate* (Fig. 6i).

### **3.3 Environmental Distribution of Ripples**

The distribution of ripple marks is conveniently discussed in terms of two principal types of environments, channels and sandflats (Allen 1968). Channels are simply open conduits through which there is a fluid flow. The flow may be constant in direction, as in rivers, or it may reverse periodically, as in tidal channels. Tidal channels range from the large channels and continuous flow of tidal estuaries, to the much smaller runoff channels encountered on sandy beaches and intertidal flats. The presence of channel walls may have some effect on ripple form by influencing the transverse uniformity of the flow. A sandflat may be a shoal between tidal channels, a broad area of the beach, or a level part of the open sea floor. Different types of ripples have been identified between varying environments. Perhaps the most significant is the predominance of two-dimensional ripples on level areas, such as sandflats, and three-dimensional ripples in channels (Allen, 1968).

### **3.4 Geological Significance**

Geologists and engineers have studied ripple marks in order to better

understand bedforms development during oscillatory flow through the integration of experimental studies that simulate wave conditions with field studies in modern nearshore settings. Such studies have been applied to bedforms preserved in ancient lacustrine and marine deposits to make quantitative estimates of paleo-depth, paleo-wave period, and paleo-wind fetch. This has been done by determining: (1) the internal structure of wave formed ripples; (2) the bottom orbital diameters required to generate specific wave-formed ripples; and (3) shallow fresh water sedimentation rates for the development of ripple marks.

Newton (1968) suggested that in most cases wave-formed ripple laminae dip toward shore, and can thereby provide a shoreline direction indicator when found in ancient sediments. The sediment transport direction may not coincide with the foreset laminae dip direction, however, cross-lamination as a sediment transport direction indicator should therefore be used with caution. Newton (1968) concluded that ripple height, wavelength and the orientation of the ripple internal structure are dependent upon both orbital diameter and the bottom oscillation velocity of the positive onshore component of the waves forming them.

Clifton and Dingler (1984) studied ripple marks to interpret ancient depositional environments. They concluded that wave-formed sedimentary structures, such as ripple marks, can be powerful interpretive tools because they reflect not only the velocity and direction of oscillatory currents, but also the length of the horizontal component of the orbital motion and the presence of velocity asymmetry within the flow. Furthermore, the ratio of ripple spacing to grain size provided an estimate of the

length of the near-bottom orbital motion. However, further field observation and experimental study must be done before wave-formed structures attain their potential for paleoenvironmental interpretation.

Using the semi-empirical formulae of Miller and Komar (1980a), and Clifton and Dingler (1984), Aspler *et al.* (1994) were able to reconstruct the hydrodynamic environment of the Hurwitz Group, Northwest Territories, Canada. It was concluded, based on calculations using wave-formed ripple marks, that the average water depth was in the range of 0.02 m to 2 m.

Geologists realize the limitations of inferences based on fossilized ripple marks in order to determine wave height, water depth, and wave period. Therefore, the assumptions and the degree of approximation involved in the different techniques impose significant constraints. Given this, further refinement of the methods used in paleoenvironmental reconstruction is needed.

### **3.5 Empirical Relationships**

Darwin (1884) was amongst the first to treat ripple marks experimentally. He suggested that small-scale ripples are due to the vortex which develops to the lee of any irregularity along the bottom. The dominant current carries sediment up the stoss slope and the vortex up the lee slope. Cornish (1934) applied this concept to aeolian and fluvial ripple marks. He maintained that these features held eddies captive to their lee, and that these eddies played a major role in controlling the shape and development of ripple marks (Fig. 1). Principally, their role was to build up the crest,

until other conditions imposed a limit to further growth, in the manner indicated by Darwin. Bagnold (1946) quantified the relationship between ripple size and flow conditions, and this work has been extended by subsequent investigations. Many aspects of oscillation ripple morphology can now be predicted.

Bagnold's experiments on oscillation ripples showed that there is a relationship between orbital diameter and ripple wavelength when flow conditions are near the threshold of grain motion. Once grains begin moving, ripples form and their wavelength is approximately equal to the orbital diameter. Increases in orbital diameter cause wavelength to increase until a limiting value is reached. This limiting value is grain size dependent. In a comprehensive field study of wave formed ripples, Inman (1957) found that ripple wavelength generally decreases with increasing orbital diameter. The Inman field data, however, were produced under larger orbital diameters than those of Bagnold's laboratory data.

Combining the data sets of Bagnold (1946) and Inman (1957) reinforces Bagnold's observation that ripple wavelength can only increase to a certain point with increasing orbital diameter. Then, rather than remain constant, as might be inferred from Bagnold's data, the wavelength actually decreases again. These aspects of ripple wavelength were integrated into a conceptual model of sediment structures by Clifton (1976).

According to Clifton (1976), ripples produced by shoaling waves can be integrated into a conceptual model based on four parameters: maximum bottom orbital velocity ( $u_m$ ), velocity asymmetry ( $\Delta u_m$ ), medium grain size ( $D$ ), and wave

period ( $T$ ). The parameters can be related to physical aspects of the environment by applicable wave theories. Analysis of ripple wavelengths,  $\lambda$ , indicate that most wave generated ripples fall into three categories, depending on the relationship between wavelength to grain size and orbital diameter ( $d_o$ ) at a given wave period. At low values of the ratio of wave orbital diameter to mean grain diameter ( $d_o/D$ ) ripple wavelength is proportional to  $d_o$ ; Clifton refers to these as orbital ripples. This type of ripple forms under short wave periods, and their wavelength depends directly on the length of the orbital diameter. At relatively large values of  $d_o/D$ , ripple wavelength depends directly on grain size and is independent of  $d_o$ . Clifton refers to these as anorbital ripples. Anorbital ripples form where orbital diameter is very large and their wavelength depends directly on grain size and is independent of the orbital diameter. A transitional range of  $d_o/D$  values exists in intermediate wave conditions in which both anorbital and orbital ripples appear possible, as well as ripples having intermediate wavelengths (suborbital ripples). Therefore, suborbital ripples form under longer wave periods, and their wavelength increases with increasing grain size and decreases with increasing orbital diameter. The wavelengths of suborbital ripples measured in the laboratory and field can differ by more than a factor of 3 at a given  $d_o/D$ . Clifton (1976) and Wiberg and Harris (1994) note that orbital ripples are the dominant type observed in laboratory studies, whereas anorbital ripples are more common in field settings.

Miller and Komar (1980b) examined the relationship between  $d_o$  and  $\lambda$  for natural ocean waves. The orbital diameter was determined from Airy wave theory:

$$d_o = H / \sinh(2\pi h / L) = u_m T / \pi \quad (1)$$

where  $H$  is the significant wave height,  $L$  is the wave length, and  $h$  is the water depth. These parameters can all be measured or calculated for simple sinusoidal laboratory waves. A problem obviously arises, however, when we attempt to measure these wave orbital parameters in the field, although where there is a well defined set of swells waves present, the Airy wave theory can still be applied with an acceptable degree of accuracy (Miller and Komar, 1980b).

Miller and Komar (1980b) collected data from a range of wave energy environments, and with grain sizes ranging from 125 to 913  $\mu\text{m}$ . All field data were compared with the empirical relationship  $\lambda = 0.65 d_o$  for orbital ripples, based upon data obtained in controlled laboratory experiments with simple oscillatory water motion (Miller and Komar, 1980a). It was concluded that the field data showed the best agreement with the laboratory results if the calculation of  $d_o$  is based upon the significant wave height  $H_{1/3}$ . Clifton and Dingler (1984) proposed that anorbital ripples occur at relatively high values of  $d_o/D$ . They have spacing that is essentially independent of  $d_o$ , but varies in roughly constant proportion to grain diameter ( $\lambda = 400$  to  $600D$ ). Wilberg and Harris (1994) compared their data with the empirical relationship  $\lambda = 0.62 d_o$  for orbital ripples, and  $\lambda = 535D$  for anorbital ripples. They suggested that ripples with spacings that fall between these relationships are considered to be suborbital ripples.

Ripple morphology is controlled by many factors, including the maximum orbital velocity and diameter near the bed, grain diameter, and possibly the period of



the waves (Allen 1979; Boyd *et al.*, 1988; Mogridge *et al.*, 1994). Numerous workers have studied ripple wavelength in the field and laboratory (Bagnold, 1946; Carstens *et al.*, 1969; Mogridge, 1972; Lofquist, 1978; Miller and Komar, 1980a; Nielsen, 1981; Kos'yan and Kochergin, 1992; Mogridge *et al.*, 1994). From their work it may be concluded that ripple wavelength and height are largely determined by the mobility number,  $\psi$ , (the ratio of the water velocity amplitude to the sediment settling velocity). More specifically, under moderate flow conditions the ripple wavelength is a constant fraction of the water semi-excursion ( $a$ ), or more precisely  $\lambda/a=1.3$  for  $\psi \leq 20$ , where the mobility number (Brebner, 1980) is defined by:

$$\psi = [a (2\pi / T)]^2 / (s - 1)gD \quad (2)$$

Where  $2\pi/T$  is the wave radian frequency,  $s$  the relative sediment density, and  $g$  the acceleration due to gravity.

Brebner (1980) attempted to model ripple wavelength using the mobility number. With sediment ranging from 100 to 550  $\mu\text{m}$  in diameter, and orbital diameters and wave periods ranging from 0.15 to 1.5 m and 3 to 15 seconds respectively, he concluded that ripples will not form unless the mobility number is greater than 3. However, if the wave period is reduced, thereby increasing the mobility number, ripple marks composed of fine grain sediments (100 to 200  $\mu\text{m}$ ) may be wiped out. On the other hand, Nielsen (1981) suggested that ripple wavelength is a very complicated function of the flow and sediment parameters, although it is of the same order of magnitude as the water semi-excursion. The single most important parameter determining  $\lambda/a$  is the mobility number. When ripple wavelength is a

fraction of the water semi-excursion, it is nearly a constant when the mobility number is less than 20. As the mobility number increasingly exceeds 20,  $\lambda/a$  decreases in such a way that  $\lambda$  decreases slowly or is a constant. Nielsen concluded that although ripples in the field obey the same rules as laboratory ripples, they are generally shorter and flatter owing to the irregularity of natural waves.

There are many field investigations on ripple morphology. The range of field measurements, however, together with adequate measurements of wave conditions, consist of fewer than the thirty data points of Dingler and Inman (1976), and the somewhat more extensive but less reliable data of Inman (1957). In addition, both workers obtained their measurements from the shallow waters off La Jolla, California, with a few points from other low-energy locations. Suggestions have been made that the predictive methods used to describe ripple wavelength should be re-examined to account for variations in wave parameters and grain size.

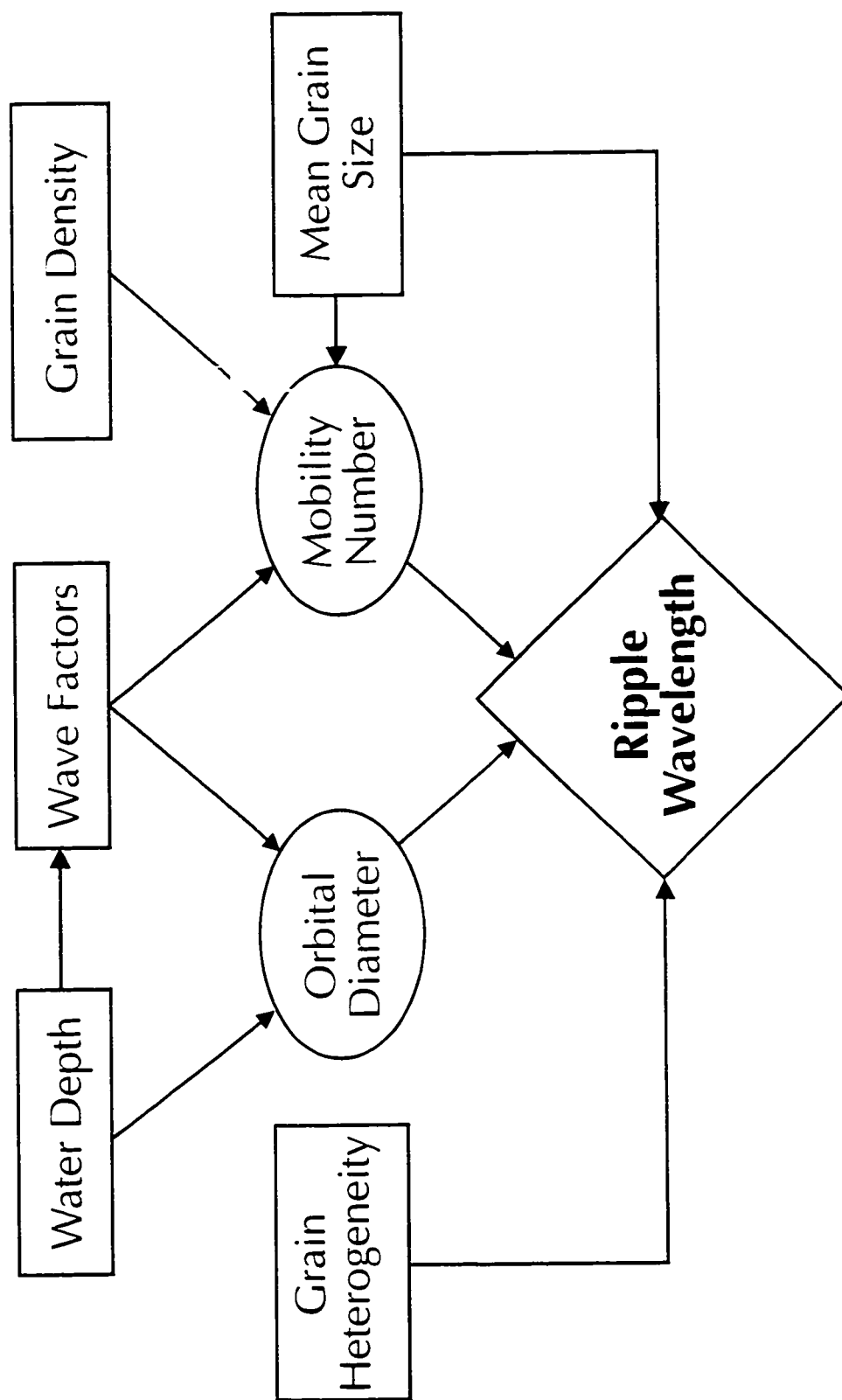
## CHAPTER 4.0

### CONCEPTUAL BASIS OF THE STUDY

An *a priori* model is a provisional representation of the real world designed to portray the problem in terms of a possible theoretical investigation. The *a priori model* developed for this study, based of the theory of ripple morphology, portrays relationships between ripple wavelength and hydrodynamic and sedimentary factors (Fig. 7). The morphology of ripples along the coast of Guyana is part of a process response system that is continuously undergoing temporal and spatial changes in form and shape. The processes affecting ripple wavelength represent responses to changes in the net transport of suspended sediment resulting from the interaction of sediments (i.e. grain density, grain heterogeneity and mean grain size) and hydrodynamic factors.

The model which will be employed for the purpose of this investigation suggests that ripple wavelengths constitute an integration of the following parameters: water depth; wave factors; and grain density, mean grain size, and grain heterogeneity (Clifton, 1976; Dingler and Inman, 1976; Allen, 1979; Miller and Komar, 1980b; Nielsen, 1981; Vongvisessomjai, 1984; Boyd *et al.*, 1988; Kawata *et al.*, 1992; Mogridge *et al.*, 1994 Wilberg and Harris, 1994). These parameters can be used to calculate the orbital diameter and mobility number. It has been suggested that ripple wavelengths are proportional to the orbital diameter in the laboratory (i.e. orbital ripples) (Clifton, 1976; Mogridge *et al.*, 1994), whereas, field experiments indicate that wavelengths are proportional to grain size and are nearly independent of orbital

## A PRIORI MODEL



Source: Author, 1996

Figure 7

diameter (i.e. anorbital ripples) (Miller and Komar, 1980b; Grant and Madsen, 1982; Boyd *et al.*, 1988; Mogridge *et al.*, 1994; Wilberg and Harris, 1994). Furthermore, there is evidence from field data that wavelength depends only on sediment size when the orbital diameter is very small (Mogridge *et al.*, 1994). Other workers have suggested that ripple wavelength can be adequately predicted by the mobility number (Berkner, 1980; Nielsen, 1981; Mogridge *et al.*, 1994).

#### **4.1 Hypotheses**

There has been no research on ripple morphology in a sand/mud environment. Furthermore, although a significant amount of research has been conducted utilizing models to describe ripple wavelength, considerable confusion and disagreement still exists. Based on the conceptual framework of the *a priori* model, review of the literature, and the objectives of the study, it is hypothesized that:

1. **There is a direct relationship between ripple wavelength and the wave orbital diameter;**
2. **The relationship between ripple wavelength and wave parameters is a function of grain diameter.**

These hypotheses illustrate general inferences promoted by several investigators. Each hypothesis can be related to the orbital diameter and the mobility number. The first hypothesis, is well recognized but has been the subject of much discussion (Inman, 1957; Dingler and Inman, 1976; Clifton, 1976; Miller and Komar, 1980b; Boyd *et al.*, 1988; Mogridge *et al.*, 1994; Wilberg and Harris, 1994). Although

it has been inferred that there is a direct relationship between ripple wavelength and orbital diameter, attempts at understanding the empirical relationships have led to a variety of opinions. The work of Berberner (1980), Nielsen (1981), and Mogridge *et al.* (1994) supports the second hypothesis. It has been inferred that there is a strong dependence between ripple wavelength and the mobility number, which is a function of grain size. However, previous workers have studied ripples with a sediment regime ranging from very fine sand (88  $\mu\text{m}$ ) to very coarse sands (1000  $\mu\text{m}$ ), whereas this investigation studied ripples with a bimodal sediment regime ranging in size from 55  $\mu\text{m}$  to 103  $\mu\text{m}$ . Therefore, the goal of this study was to collect ripple data in an environment with much fine sediment than in the studies of Inman (1957), Dingler and Inman (1976), and Miller and Komar (1980b).

## CHAPTER 5.0

### METHODOLOGY

To test the stated hypotheses, it was necessary to measure ripple wavelengths, mean grain size, water depth, wave height, and wave period in the field; these data are referred to as the primary data set. These data were obtained from measurements taken at 11 randomly selected sampling sites on the study beach for the period June 16 to July 6, 1994 (Fig. 8). The study beach was surveyed using horizontal and vertical measurements based upon standard levelling methods, with readings taken at the shoreline and at all significant changes in elevations.

Traditionally, ripple marks have been described in terms of their vertical and longitudinal profiles (Fig. 9). The vertical interval between the crest and trough is the ripple *height* while the horizontal distance between them is the ripple *wavelength* or *chord*. The profile of figure 9a is characteristic of many ripples, in that the point of maximum elevation lies a little way back from the top of the slipface. The second profile, seen in figure 9b, is more characteristic of ripples formed in shallow water, where the ripple crest becomes planed down to a flat surface. In these cases the summitpoint is at the top of the slipface. Descriptive terms used to define ripples, as described by Allen (1968), can be reviewed in Appendix I.

Ripple wavelengths were obtained by measuring two sets of three ripples each, yielding one mean wavelength for each of the eleven study sites. Wavelengths were measured using a standard 30 cm ruler with a margin of error of approximately

# SAMPLING STATIONS

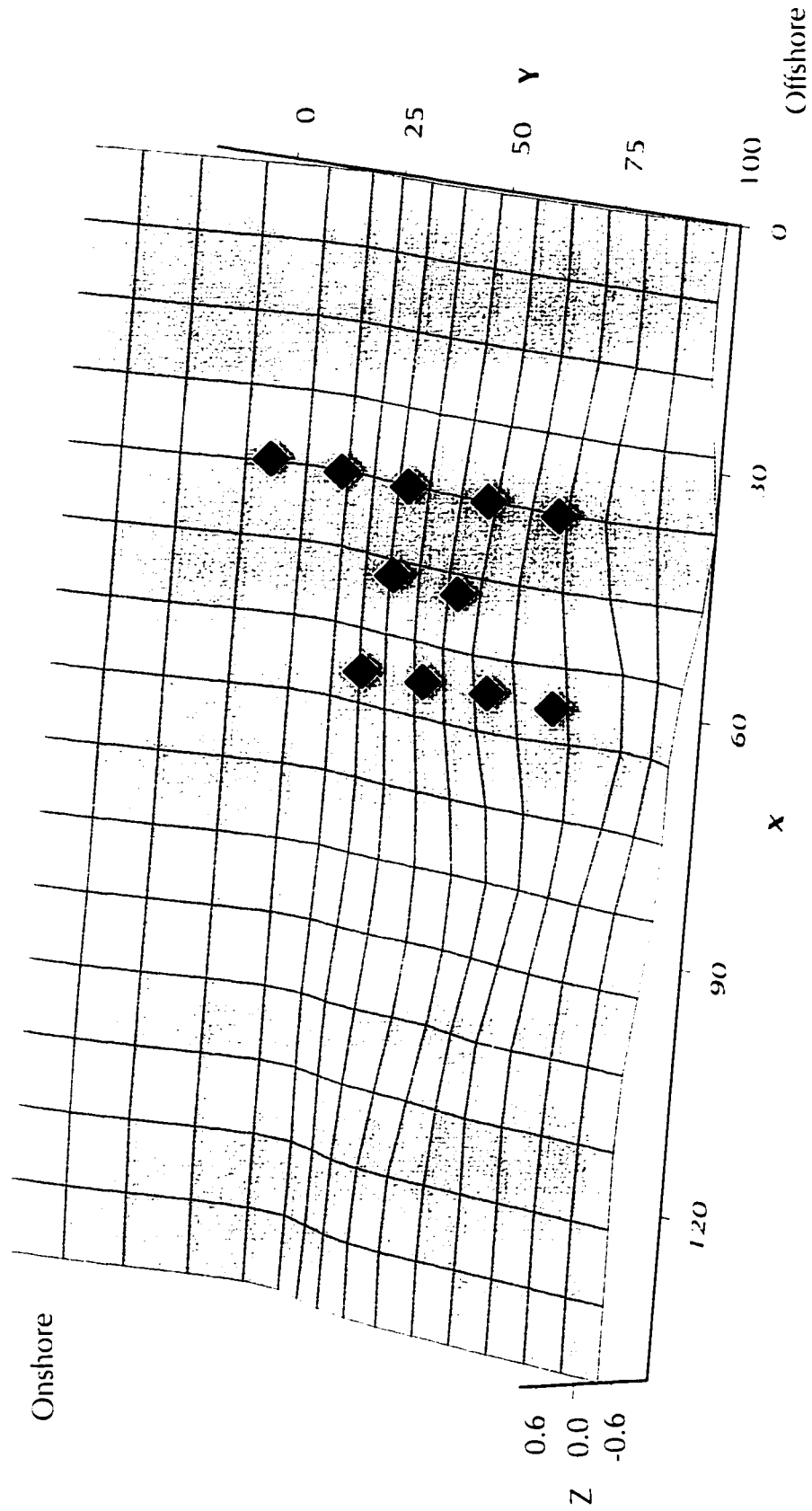


Figure 8

Source: Author, 1996

Note: All values are in meters.



## Ripple Marks in Profile

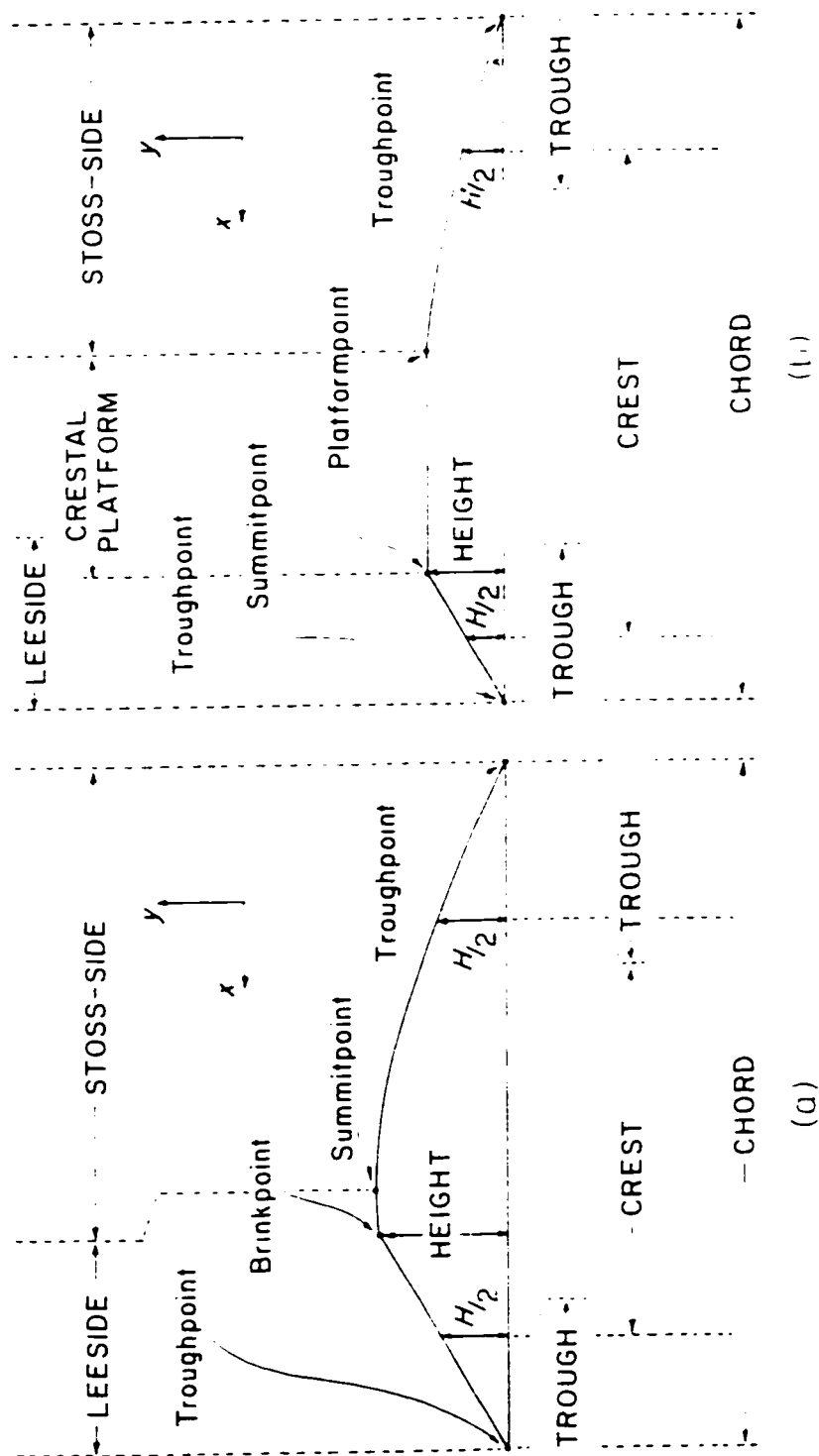


**Figure 9:** The X coordinate is parallel to flow, and the Y coordinate is the vertical axis (Source: Allen, 1969).

$\pm 1$  mm. Each study site, using the method employed above, represented a stratified random sample. These types of samples are best employed when dealing with complex heterogeneous populations. The key to the use of the stratified random sample design is on the efficient employment of a good classification which subdivides the population into homogeneous subpopulations, and that the rules which govern them are applied.

Numerous wave generated motions including mass transport, undertow and infragravity currents, co-exist and interact in a complex way in the surf and nearshore zones. These currents, however, tend to be weak along the bottom. Waves generate onshore, offshore motions, and therefore unlikely to have contributed significantly to bottom current velocities. Given this, maximum bottom orbital velocities were obtained using a portable electromagnetic flowmeter. This device operates under the Faraday Principle, in which a conductor (such as water) moves through the device's sensor and cuts the lines of the magnetic flux. This disruption produces a voltage directly proportional to the velocity at which the conductor moves through the magnetic field (Marsh-McBirney Inc., 1990). Its accuracy is considered to be  $\pm 2$  percent of the recorded readings. The device was oriented parallel and perpendicular to the shoreline, at eighty percent of the water depth (top-down), to determine the maximum bottom orbital velocity at each of the eleven sites.

Both trough and crest sediment samples were collected at each of the eleven sites. Grain size analyses were carried out by using the Brinkman 2010 Particle Size Analysis (PSA) system. This system provides fast and accurate particle size data using

a laser-based analyser. The system employs the Time-of Transition theory, which states that the time it takes a particle to cross a laser beam moving at a fixed velocity depends on the particle's diameter (Brinkman Instruments Inc., 1988). Thus, particle-laser interactions can be processed to yield diameter size. The PSA system provides statistical data on the following parameters: diameter; volume; number of particles sampled and concentration. The results of the analyses are printed in graphic and tabular forms.

The importance of wave height, wave period, and water depth on coastal processes is well documented. During the study period, supplementary data on wave height, wave period, and water depth were determined daily. Analysis of these data is necessary in order to determine whether a constant steady sea state existed. Wave height and water depth were determined using a standard calibrated wave staff at each of the eleven sample sites. Similarly, measurements of wave periods were made using a stopwatch.

To evaluate the first hypothesis, that a direct relationship exists between ripple wavelength and the wave orbital diameter, an independent Pearson Correlation and Regression test was employed on the data. Such a test can evaluate the first hypothesis, in that some dependent variable  $Y$  (ripple wavelength) is functionally related to an independent variable  $X$  (wave orbital diameter), and this relationship can be described by a straight line on a two variable graph. However, six assumptions associated with this type of analysis must first be met. The first indicates that the regression analysis fits a straight line trend through a scatter of data points,

and the correlation analysis test for the goodness of fit of this line. If this assumption is not met, it is often possible to transform the data. Normality, the second assumption, states that the raw data need not be normally distributed, but that the conditional distributions of the residuals are normal. The third assumption, means of the conditional distributions, states that for every value of  $X$ , the mean of  $(Y_i - \bar{Y})$  must be zero, if it is not, the regression equation may be biased. The fourth, homoscedascity, means there is equal variance in the conditional distributions. If these are not equal, the regression equation coefficients may be severely biased. Autocorrelation assumes that the value of each observation on the independent variable is independent of all of the values of the others, so that one cannot predict the value of  $X$ . The final assumption assumes that both  $X$  and  $Y$  are measured without error (Johnston, 1980).

The first hypothesis was tested by plotting measured ripple wavelengths normalized by grain diameter (i.e.  $\lambda/D$ ), as a function of the normalized wave orbital diameter (i.e.  $d_o/D$ ). Normalizing the data with grain diameter is not a perfect discriminator, but is adequate for showing the general distribution of ripple types (Nielsen, 1981; and Wilberg and Harris, 1994). Therefore, this allowed the likelihood of orbital, anorbital, and suborbital ripples forming on the site under investigation to be determined. Secondly, the first hypothesis was tested by plotting ripple wavelength normalized by the water semi-excursion ( $\lambda/a$ ) as a function of normalized wave orbital diameter ( $d_o/D$ ). Nielsen (1981) concluded that the ripple wavelength is normally of the same order of magnitude as the water semi-excursion ( $\lambda/a$ ) and varies slowly with

the flow parameters.

To test the second hypothesis, whether the relationship between ripple wavelength and wave parameters is a function of grain diameter, an independent Pearson Correlation and Regression tests was employed on the data. This was used to determine if there was a strong relationship between ripple wavelength and the mobility number. Review of the literature indicates that ripple wavelength is proportional to the water semi-excursion ( $\lambda/a$ ) when the mobility number is less than about 20. Nielsen (1981) suggested that in any dimensional analysis and empirical work one should consider the ripple wavelength in terms of  $\lambda/a$  instead of  $\lambda/D$  as favoured by the literature. Therefore, it will be determined if any correlation exists between  $\lambda/a$  (dependent variable) and the mobility number (independent variable).

## CHAPTER 6.0

### BEDFORM TYPES

A total of 58 observations were made on ripple wavelength and form. During these observations, measurements were made during high tide to record maximum bottom orbital velocities, and during low tide to record ripple form and wavelength. Each ripple type was identified at each of the recording stations during the investigation. Striking changes in ripple form and wavelength occurred from day to day throughout the 58 observations. Ripple type was classified on the basis of plan shape, which ranged from straight, sinuous, linguoid, to catenary forms. The main features used to differentiate ripple type were the nature of the crest, wavelength, orientation and sinuosity. In order to make the description of forms less subjective, this investigation adopted the idealised ripple train classification system devised by Allen (1968).

#### ***Type I: Straight Ripple-trains***

Numerous different ripple-trains can be grouped under this classification. The crestlines of these ripples may either be swept relative to the flow or have the more usual transverse relationship. Straight ripple-



**Figure 10:** Straight Transverse Ripples

trains composed of small-scale two-dimensional transverse and swept ripples, constituting 95% of all ripples observed during this investigation, are shown in Figs. 10 and 11 respectively. Generally these ripples have wavelengths between 3-10 cm, with heights ranging between 0.3-1.3 cm, and they are parallel (straight) or sub-parallel (swept) to the coast. The ripples are very uniform in height, and they have a narrow crestal shoulder above a sharp brinkline. Ripple-trains of this sort are widely reported on tidal flats affected by shoaling waves or gentle tidal flows (Allen, 1968; Boyd *et al.*, 1988; Osborne *et al.*, 1993; Makino, 1994; and Wiberg and Harris, 1994). Allen (1968) believes that straight ripples are produced only by shoaling waves that generate an asymmetrical oscillatory motion at the bed. Although this is true in many cases but is not applicable generally, trains of straight-crested ripples have been observed during this investigation in the ebb flow drainage channel unaffected by surface waves. Boyd *et al.* (1988) suggested that these ripples occur only during the highest energy conditions.

Swept ripples (Fig. 11) are comparatively rare and are characteristic of straight crestlines lying at an angle, usually less than 50° (Allen, 1968). Swept ripples are generally the product of moderately strong longshore currents.

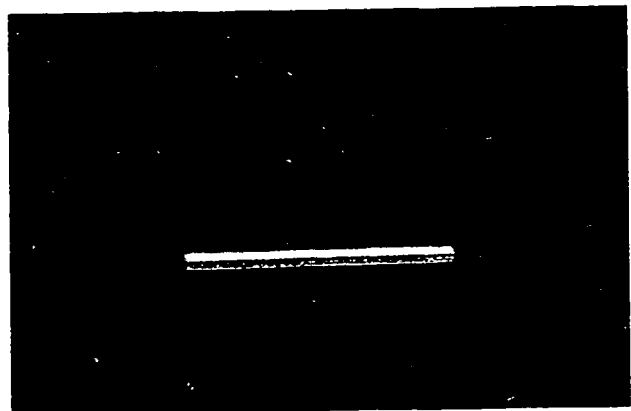


**Figure 11: Swept Ripples**

### ***Type II Sinuous Ripple-trains***

These ripples are characterized by irregular crests and numerous crest singularities. Lobes develop occasionally on the ripple crests (Figs. 12 and 13), sometimes leading to bifurcation.

Ripples of this type may be arranged in phase, however, they are largely out of phase. Sinuosity is high and the wavelength is short ranging between 3-7 cm, with heights ranging between 0.3-0.6 cm with the greatest heights at the lobes.

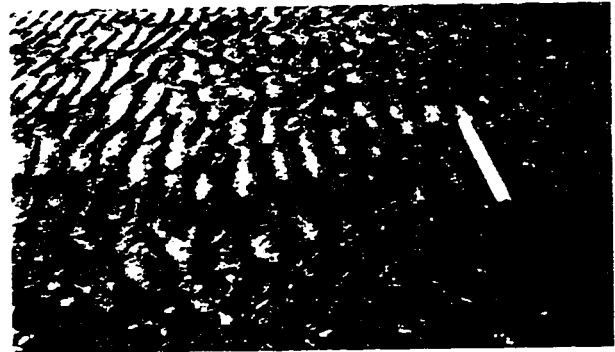


**Figure 12:** Transverse Sinuous Ripples in Phase

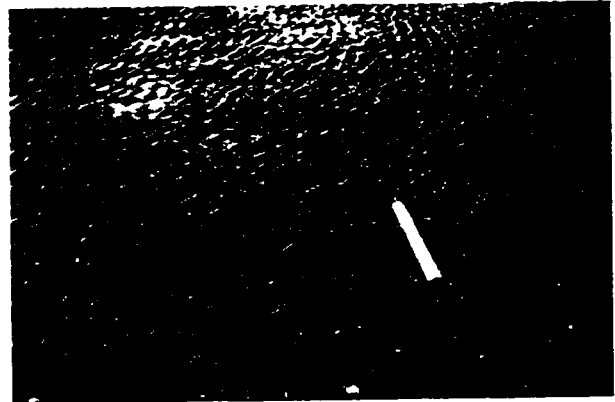


**Figure 13:** Transverse Sinuous Ripples out of Phase

Allen (1968), and Boyd *et al.* (1988) noted that there appears to be a complete gradation between two-dimensional straight ripples arranged transversely to flow and three-dimensional sinuous ripples.

### ***Type III Linguoid Ripple-trains***

Type III ripples were only identified in the trough of the study site, and their morphology was the result of high energy ebb flow drainage (a unidirectional flow much like a river), with a wave occasionally travelling back up the trough. Linguoid ripples display a greater range of form than any other ripple type. These ripples (Fig.



14) generally have rounded crests with a forward or backward closure. Ripples of this type are very uniform in size and are typically arranged out of phase, with wavelengths ranging between 4-7 cm and heights ranging between 0.4-0.6 cm.

#### ***Type IV Catenary Ripple-trains***

These ripples are characterized by an irregular crest pattern and high sinuosity (Fig. 15). They exhibit a wide range of wavelengths (4-10 cm) with heights too small to record with any accuracy. According to Body *et al.* (1988) these ripples typically exist only briefly during dramatic reorganizations of the bed, and are associated with high energy wave events and frequently are accompanied by high concentrations of suspended sediment. These ripples were



**Figure 14: Linguoid Ripples**



**Figure 15: Catenary Ripples**

only located on top of the bar at the midsurf position at high tide. They experienced high energy wave events during high tide, and strong, unidirectional drainage into the trough during low tide.

## CHAPTER 7.0

### RESULTS AND DISCUSSIONS

Analysis of ripple wavelength presents special problems since natural oscillations in the field are generated by a spectrum composed of many frequencies rather than the single used in laboratory experiments. For the purpose of this investigation it is assumed that all ripples were formed under the deepest water level at high tide, except in the trough, where they were the result of a fast ebb flow drainage. The mean ripple wavelength was 6.2 cm, ranging between 3.7 and 9.7 cm, and with a standard deviation of 1.41. Mean ripple height was 0.50 cm, ranging between 0.19 and 1.00 cm, with a standard deviation of 0.2 (Table 1).

#### 7.1 Assessment of Hypothesis #1

The first hypothesis attempted to determine if a relationship exists between ripple wavelength and wave orbital diameter. Two independent test were carried out to evaluate this hypothesis. The first was used to discover if any relationship exists between  $\lambda/D$  and  $d_o/D$ , and to determine the likelihood of orbital, suborbital, and anorbital ripples forming on the site under investigation. The second test determined if any relationship exists between  $\lambda/a$  and  $d_o/D$ . The data from this investigation have been plotted in figures 17, and 18 in the dimensional form of  $\lambda/D$  versus  $d_o/D$ , and  $\lambda/a$  versus  $d_o/D$  respectively.

Two disparate views exist regarding the relationship between  $\lambda/D$  and  $d_o/D$ .

**Table 1.** Ripple and Wave data collected off Melaine Beach, Guyana, South America  
 Note:  $N/a_{\text{predicted}}$  calculated using equation 7 ( $N/a=1419.06d_f/D^{0.972}$ ), and S=suborbital with A=anorbital

Day-Site	$h$ (cm)	$T$ (sec.)	$D$ (cm)	$H$ (cm)	$\lambda$ (cm)	$\eta$ (cm)	$d_r$ (cm)	$a$ (cm)	$\psi$	$ND$	$d_f/D$	Classification	$N/a$	$N/a_{\text{pred}}$
01-01	30	4.90	.0062	22	7.4	.59	23.40	11.70	2244.3	1193.5	3773.5	S	.63	.47
01-02	65	4.90	.0063	22	8.5	.84	18.72	9.36	1413.5	1349.2	2970.8	S	.91	.60
01-03	56	4.90	.0067	22	8.5	.43	68.63	34.31	17869.	1268.6	10242	A	.25	.18
01-04	12	4.90	.0084	22	6.1	.23	42.11	21.06	5367.0	726.19	5013.3	A	.29	.36
01-05	18	4.90	.0072	22	5.8	.26	21.84	10.92	1683.5	805.56	3032.7	S	.53	.59
01-06	60	4.90	.0065	22	5.2	.32	21.84	10.92	1864.8	800.00	3359.3	S	.48	.53
02-01	40	6.35	.0062	37	7.7	.44	22.23	11.12	1206.9	1241.9	3586.1	S	.69	.50
02-02	35	6.35	.0063	37	6.7	.69	46.49	23.24	5192.8	1063.4	7379.2	A	.29	.25
02-04	10	6.35	.0084	37	4.8	.28	119.25	59.63	25627	571.43	14197	A	.08	.13
03-01	50	7.15	.0062	42	6.7	.33	27.31	13.66	1436.3	1080.6	4405.0	S	.49	.41
03-02	50	7.15	.0063	42	7.3	.50	54.62	27.31	5654.2	1158.7	8670.1	A	.27	.21
03-03	25	7.15	.0067	42	7.1	.78	22.76	11.38	923.03	1059.7	3396.8	S	.62	.52
03-04	15	7.15	.0084	42	8.9	.68	50.07	25.04	3563.3	1059.5	5960.7	A	.36	.30
04-01	50	7.75	.0062	58	7.3	.39	51.80	25.90	4398.8	1177.4	8355.6	A	.28	.22
04-02	35	7.75	.0063	58	7.4	.52	49.34	24.67	3926.5	1174.6	7831.4	A	.30	.23
04-03	35	7.75	.0067	58	9.0	.63	51.80	25.90	4070.5	1343.2	7732.0	A	.35	.24
04-04	35	7.75	.0084	58	7.7	.27	71.54	35.77	6191.6	916.67	8516.6	A	.22	.21
04-05	45	7.75	.0072	58	6.5	.20	44.40	22.20	2782.9	902.78	6167.2	A	.29	.29
05-01	50	8.15	.0062	50	8.6	.58	36.32	18.16	1955.0	1387.1	5857.9	A	.47	.31
05-02	42	8.15	.0063	50	7.4	.52	64.86	32.43	6135.2	1174.6	10294	A	.23	.18
05-03	45	8.15	.0067	50	5.0	.28	77.83	38.91	8307.2	746.27	11615	A	.13	.16
05-09	40	8.15	.0067	50	5.3	.32	51.88	25.94	3692.1	791.04	7743.9	A	.20	.24
05-10	38	8.15	.0072	50	3.7	.28	38.91	19.46	1932.5	513.89	5404.6	A	.19	.33
06-01	50	8.00	.0062	38	6.5	.66	56.02	28.01	4827.7	1048.3	9035.8	A	.23	.20
06-02	48	8.00	.0063	38	5.2	.61	45.84	22.92	3180.4	825.40	7275.6	A	.23	.25
06-08	50	8.00	.0069	38	4.9	.72	53.48	26.74	3952.5	710.14	7750.1	A	.18	.24
06-09	54	8.00	.0067	38	4.1	.50	56.02	28.01	4467.4	611.94	8361.5	A	.15	.22
06-10	60	8.00	.0072	38	4.8	.23	38.20	19.10	1932.5	666.67	5305.1	A	.25	.34
07-01	30	6.75	.0062	29	5.1	.54	21.49	10.74	997.46	822.58	3465.4	S	.47	.51

**Table 1 (con't).** Ripple and Wave data collected off Melaine Beach, Guyana, South America  
 Note:  $N/a_{\text{predicted}}$  calculated using equation 7 ( $N/a=1419.06d_p/D^{0.972}$ ), and S=suborbital with A=anorbital

Day-Site	h (cm)	T (sec.)	D (cm)	H (cm)	$\lambda$ (cm)	$\eta$ (cm)	$d_p$ (cm)	a (cm)	$\psi$	N/D	$d_p/D$	Classification	N/a	$N/a_{\text{pred}}$
07-02	25	6.75	.0063	29	29	.53	25.78	12.89	1413.5	666.67	4092.5	S	.33	.44
07-03	30	6.75	.0067	29	29	.20	45.14	22.57	4070.5	865.67	6737.3	A	.26	.27
07-08	45	6.75	.0069	29	29	.88	25.78	12.89	1290.6	753.62	3736.6	S	.40	.48
07-09	38	6.75	.0067	29	29	.83	15.04	7.52	452.28	925.37	2244.8	S	.82	.78
07-10	40	6.75	.0072	29	29	.54	45.12	22.56	3787.8	680.56	6266.7	A	.22	.29
08-01	27	7.40	.0062	28	28	.72	14.13	7.07	359.09	758.06	2279.5	S	.67	.77
08-02	15	7.40	.0063	28	28	.42	40.04	20.02	2836.9	730.16	6356.0	A	.23	.29
08-03	20	7.40	.0067	28	28	.51	44.75	22.38	3332.1	910.45	6679.7	A	.27	.27
08-08	20	7.40	.0069	28	28	.43	28.27	14.13	1290.6	1043.4	4096.5	S	.51	.44
08-09	30	7.40	.0067	28	28	.83	30.62	15.31	1559.9	865.67	4570.3	S	.38	.39
08-10	28	7.40	.0072	28	28	.58	21.20	10.60	695.73	722.22	2944.3	S	.49	.60
09-01	5	7.40	.0062	38	38	.27	16.49	8.24	488.76	1000.0	2659.4	S	.75	.67
09-02	20	7.40	.0063	38	38	.30	37.69	18.84	2512.9	761.90	5982.2	A	.25	.30
09-09	12	7.40	.0067	38	38	.51	7.07	3.53	83.07	850.75	1054.7	S	1.61	1.64
09-10	10	7.40	.0072	38	38	.67	35.33	17.67	1932.5	736.11	4907.2	S	.30	.37
10-01	80	7.55	.0062	40	40	.31	28.84	14.42	1436.3	1225.8	4651.4	S	.53	.39
10-02	15	7.55	.0063	40	40	.60	43.26	21.63	3180.4	1396.8	6866.4	A	.41	.26
10-09	15	7.55	.0067	40	40	1.00	19.23	9.61	590.74	1000.0	2869.5	S	.70	.62
10-10	10	7.55	.0072	40	40	.47	16.82	8.41	420.87	666.67	2336.4	S	.57	.75
11-01	17	8.05	.0062	45	45	.36	41.00	20.50	2553.5	1096.7	6612.6	A	.33	.27
11-02	12	8.05	.0063	45	45	.35	64.06	32.03	6135.2	1539.6	10168	A	.30	.18
11-03	10	8.05	.0067	45	45	.37	56.37	28.19	4467.4	910.45	8413.8	A	.22	.22
11-09	20	8.05	.0067	45	45	.84	30.75	15.37	1329.1	880.60	4589.3	S	.38	.39
11-10	15	8.05	.0072	45	45	.74	33.31	16.66	1451.5	888.89	4626.5	S	.38	.39
12-01	13	8.40	.0062	60	60	.47	58.82	29.41	4827.7	693.55	9487.6	A	.15	.19
12-02	15	8.40	.0063	60	60	.19	45.45	22.73	2836.9	825.40	7215.0	A	.23	.25
12-06	15	8.40	.0065	60	60	.35	61.50	30.75	5033.0	800.00	9461.1	A	.17	.19
12-09	20	8.40	.0067	60	60	.65	45.45	22.73	2667.5	850.75	6784.2	A	.25	.27
12-10	20	8.40	.0072	60	60	.43	48.13	24.06	2782.9	736.11	6684.5	A	.22	.27

Inman (1957) suggested that for a given grain size,  $\lambda D$  is directly proportional to  $d_o/D$  until some critical maximum  $d_o/D$  value is reached. Spacing then becomes inversely proportional to  $d_o/D$ , until it diminishes and ultimately reaches a constant intermediate value. Dingler (1974) plotted Inman's (1957) field data and original laboratory measurements and found a similar relationship. In contrast, Allen (1979), after plotting a large amount of existing data (mostly laboratory), found no well-defined relationship between  $d_o/D$  and  $\lambda D$  for a given size of sand. He therefore concluded that Inman's bell-shaped curve was spurious (Fig. 16). Miller and Komar (1980a) analysed much of the same data and concluded that differences in the data sets could be attributed to the type of laboratory device used to generate the oscillatory motions. In particular, the results of oscillating bed experiments, which dominate Allen's data, are different from water-tunnel, wave-channel, and presumably, field results. Therefore, oscillating bed experiments indicate that, for a given grain size,  $\lambda D$  increases with  $d_o/D$  until it reaches a maximum and then remains constant.

When  $\lambda D$  is plotted against  $d_o/D$  (Fig. 17) the data show no clear relationship ( $r^2=0.0032$ ) (refer to Appendix II for statistical results). This however, does not mean that we cannot classify the observed ripples. For example, Fig. 16 is a dimensionless plot of  $\lambda D$  against  $d_o/D$  for a number of field and laboratory studies. The field data tend to dominate the right side of the diagram (high  $d_o/D$  values), whereas laboratory experiments dominate the plot at low  $d_o/D$  values. As might be expected, the field data are more broadly scattered, but both sets of data show a bell-shaped relationship. Various investigators have subdivided ripples into three types based on the

## Classification of Ripples Based on the Relationship Between $\lambda/D$ as a Function of $d_o/D$

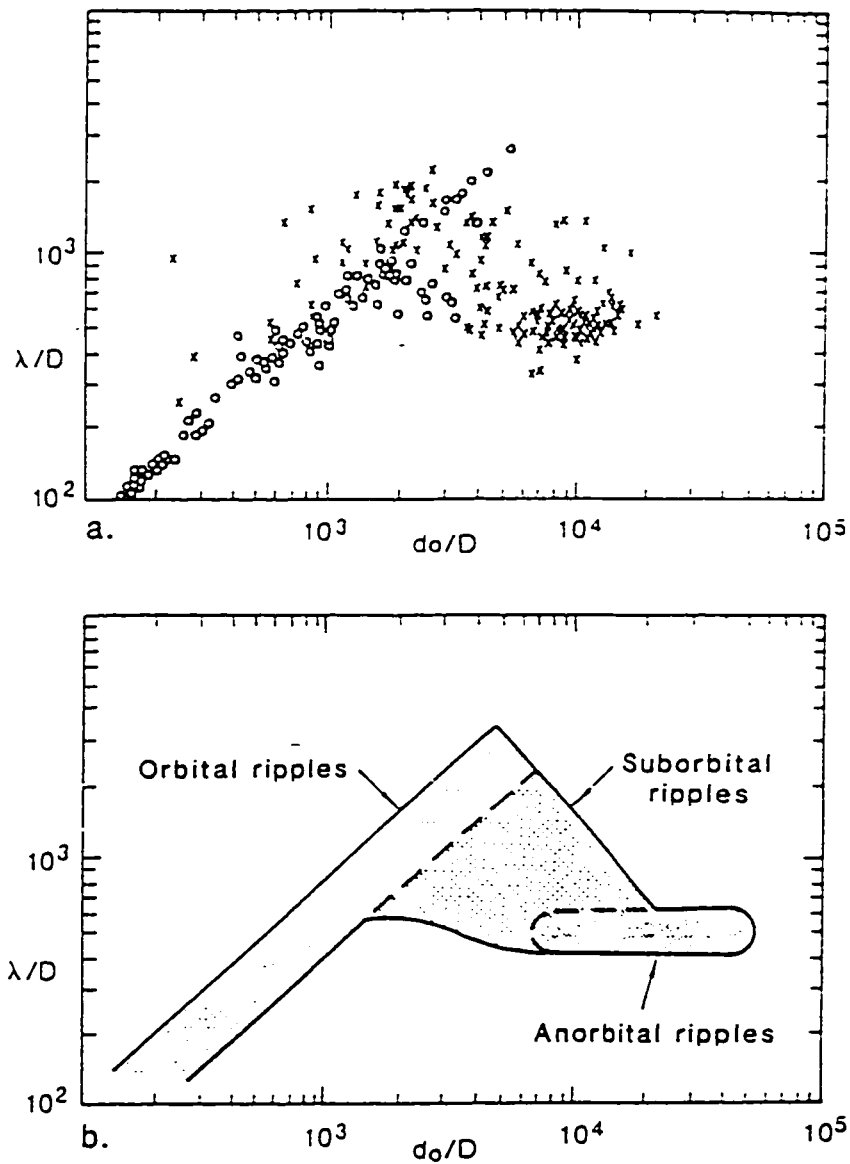


**Figure 16(a) and (b):** Plot of ripple wavelength normalized by grain size  $\lambda/D$ , as a function of normalized orbital diameter  $d_o/D$  (Fig. 16a). Data included field observation from Inman (1957), Dingler (1974), Miller and Komar (1980b), and Clifton and Dingler (1982). Laboratory observations included those of Carstens *et al.* (1969), Mogridge and Kamphuis (1972), and Miller and Komar (1980a). Figure 16b illustrates the classification of ripples based on the distribution shown in figure 16a. (Source: Clifton and Dingler, 1984)

relationship between ripple spacing and orbital diameter. This subdivision (Fig. 16b) appears to be valid for the data set presented (Fig. 17).

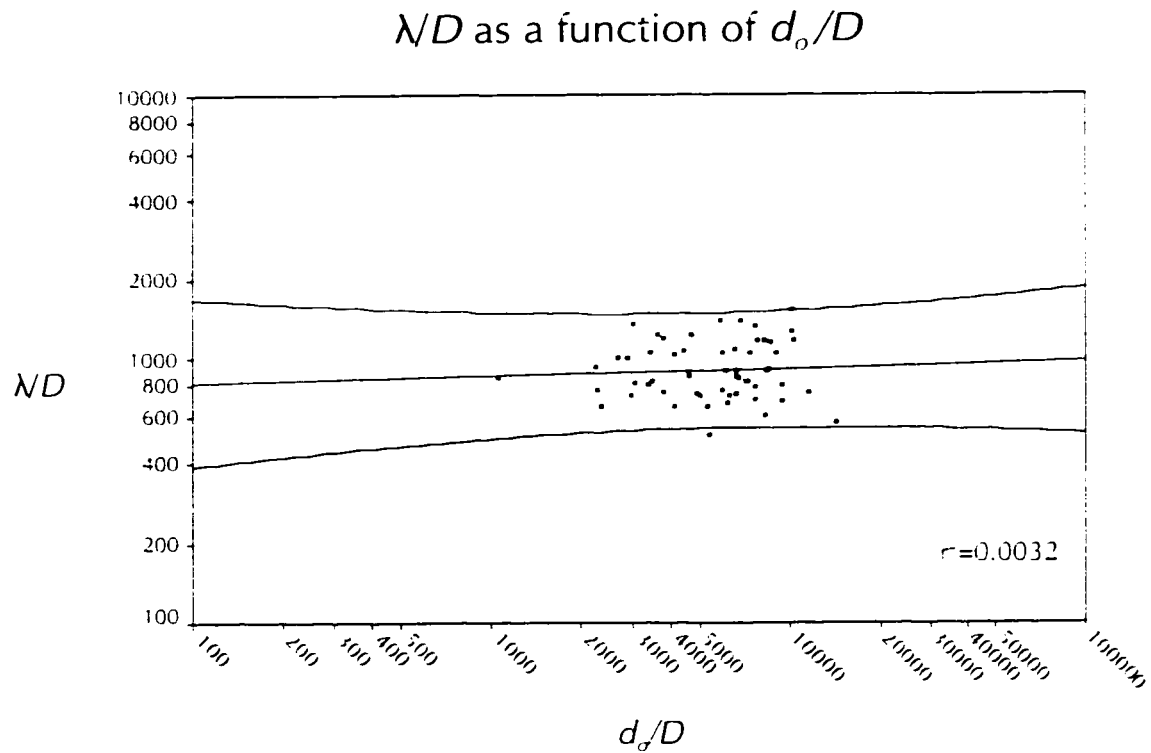


**Figure 17:** Measured ripple wavelength ( $\lambda$ ) normalized by grain diameter ( $D$ ), as a function of normalized orbital diameter ( $d_o/D$ ), using the methods described by Miller and Komar (1980a).

“Orbital ripples” are those on the left side of Fig. 16b where  $\lambda/D$  is proportional to  $d_o/D$  in the approximate relationship  $\lambda=0.65d_o$  (Miller and Komar 1980a). Such ripples can form under conditions where the  $d_o/D$  ratio lies in the range of 100-3000 or more (Fig. 16b). Their spacing to grain size ratio ( $\lambda/D$ ) ranges from less than 100 to more than 2000. Because of the requirement for short oscillatory motion, orbital ripples occur most commonly in very shallow water under short-period waves (Clifton and Dingler, 1984). The spacing of orbital ripples tends to increase in a shoreward

direction, parallelling the increase in  $d_o$  as a wave shoals (Komar, 1974), and the spacing appears to be independent of grain size.

Ripple spacing remains proportional to orbital diameter until the  $d_o/D$  ratio reaches the range of 1000-5000 (Clifton, 1976, and calculations from Miller and Komar, 1980a). Under such conditions (Fig. 16b), ripple spacing decreases as orbital diameter increases. Ripples formed under these conditions were accordingly termed “suborbital” (Clifton 1976). Ripple spacing appears to depend both on orbital diameter and grain size in some undefined relationship.

At  $d_o/D$  values in excess of 5000, ripple spacing stabilizes at a value that is independent of orbital diameter (Fig. 16b). Termed “anorbital ripples” by Clifton (1976), such ripples are most commonly observed in fine sand where they have spacings of 5-10 cm. Typically their  $\lambda/D$  ratio lies in the range of 400-600 under conditions of a single train of waves. Recent field studies indicate that, under a polymodal wave spectrum (more than one wave train present), the spacing to grain size ratio of anorbital ripples may be on the order of 1200 (Miller and Komar, 1980b). Anorbital ripples are probably the only type to form in fine sand under very long period (>12 s) waves. Clifton and Dingler (1984) suggested that anorbital ripples, which occur at relatively high values of  $d_o/D$ , have spacings that are essentially independent of  $d_o$ , and vary in roughly constant proportion to grain diameter. They proposed that for anorbital ripples:

$$\lambda \approx 400D \sim 600D \quad (3)$$

Although no relationship was found to exist between  $\lambda/D$  and  $d_o/D$  (Fig. 17),



comparing the results of this investigation to Fig. 16b, we can infer that the majority of the observed ripples may be classified as **suborbital** (40%) and **anorbital** (60%). According to Miller and Komar (1980a), oscillating bed experiments indicate that, for a given grain size,  $\lambda/D$  increases with  $d_o/D$  until it reaches a maximum and then remains constant: this may very well be the case with the observed data. Under the conditions observed (multichromatic waves),  $d_o/D$  values range between 1054 and 14 197, with a mean value of 6070,  $\lambda/D$  values range between 514 and 1540, with a mean value of 930, and average ripple wavelength ranged between 3.7 and 9.7 cm. The observed values of  $d_o/D$  and  $\lambda/D$  are on average higher than those observed by previous investigators. Most work has been conducted on grain sizes  $>125\mu\text{m}$ , however, while this investigation was concerned with sediments ranging in size between 55.8 and 103.6 $\mu\text{m}$ . This investigation suggests that the relationship which best describe anorbital ripples, derived from the data in Table 1, in a sand/mud environment is:

$$\lambda \approx 514D \sim 1540D \quad (4)$$

The second test confirmed Nielsen's (1981), Grant and Madsen's (1982), and Wiberg and Harris's (1994) relationships for ripples utilizing the water semi-excursion ( $a$ ). Nielsen (1981) concluded that ripple length is normally of the same order of magnitude as the water semi-excursion, and under gentle flow conditions the ratio  $\lambda/a$  varies with the flow parameters. When  $\lambda/a$  was plotted against  $d_o/D$  the data showed a strong inverse relationship with  $r^2=0.7936$ , and  $r=-0.891$  (Fig. 18) (refer to Appendix

### $\lambda/a$ as a function of $d_o/D$

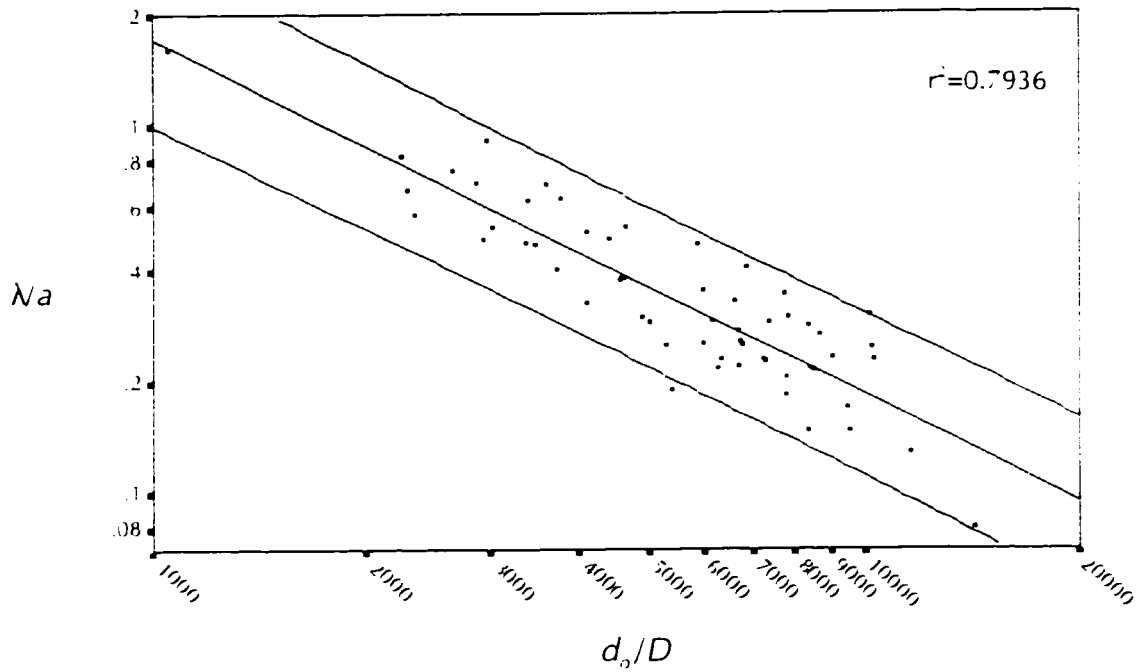


**Figure 18:** Measured ripple wavelength ( $\lambda$ ) normalized by the water semi-excursion ( $a$ ), as a function of normalized orbital diameter ( $d_o/D$ ).

II for statistical output). The results of the second test, for ripple wavelength as a function of orbital diameter are compared to the work of Nielsen (1981), Grant and Madsen (1982), and Wiberg and Harris (1994) (Fig. 19). Comparisons are shown for wave periods of  $T=3.5$  s and  $T=10$  s, which are representative of laboratory and field conditions. Nielsen's (1981) laboratory expression (5) were used when  $T=3.5$  s:

$$\lambda/a = 2.2 - 0.345\psi^{0.34} \quad (5)$$

and his field relationships (6) were used when  $T=10$  s:

$$\lambda/a = \exp[(693 - 0.37\ln^8\psi)/(1000 + 0.75\ln^7\psi)] \quad (6)$$

Based on estimates of critical shear stress for initial motion and for full suspension of  $210\mu\text{m}$  quartz sand, the range of values of  $d_o/D$  for bed load transport is roughly 900-

3000 when  $T=3.5$  s; if  $T=10$  s, the range of  $d_o/D$  is roughly 3000-10 000. These ranges define the conditions under which ripples would be active, and indicate that with  $T=3.5$  s ripples are orbital and suborbital, whereas with  $T=10$  s ripples are suborbital and anorbital (Wiberg and Harris, 1994). However, this investigation observed an average  $T=7.3$  s, with  $d_o/D$  values ranging between 1054 and 14 197. This range defines the conditions, in a sand/mud environment, in which ripples would be active and classified as suborbital and anorbital. Thus ripple wavelengths are completely specified given  $a$ , and  $D$ .

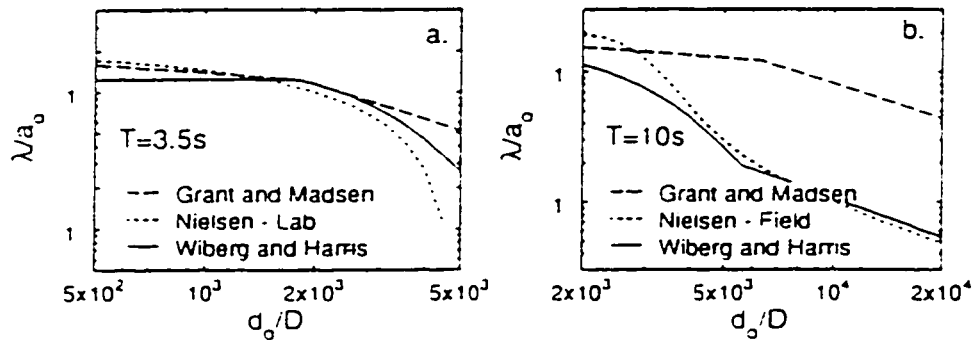


**Figure 19:** Comparison of the predicted relationships for (a, b) ripple wavelength, normalized by the water semi-excursion (a) as a function of  $d_o/D$  computed using the methods of Nielsen (1981), Grant and Madsen (1982), and Wiberg and Harris (1994). (Source: Wiberg and Harris, 1994)

The results of Nielsen (1981), Grant and Madsen (1982), and Wiberg and Harris (1994) are similar to those in this investigation although the empirical formulae are different in this study. The results of this analysis suggest, as others have noted, that ripples observed in the field may be interpreted within a common framework. This framework provides a method for classifying ripples as orbital, suborbital or

anorbital based on orbital diameter, the water semi-excursion, and grain size, and for predicting ripple wavelength based on ripple type and flow characteristics . The field relationship (7), derived from the regression line in Fig. 18, attempts to construct a more general method for predicting ripple wavelength.

$$\lambda/a = 1419.06 d_o/D^{-0.972} \quad (7)$$

With an average wave period of  $T=7.3$  s, and sediments ranging in grain size between 55.8 and 103.6  $\mu\text{m}$ , the results of correlating  $\lambda/a_{\text{predicted}}$  from equation (7) against  $\lambda/a_{\text{measured}}$ , provided a  $r^2=0.8664$ , and a  $r=0.931$  (Fig. 20) (refer to Appendix II for statistical results).

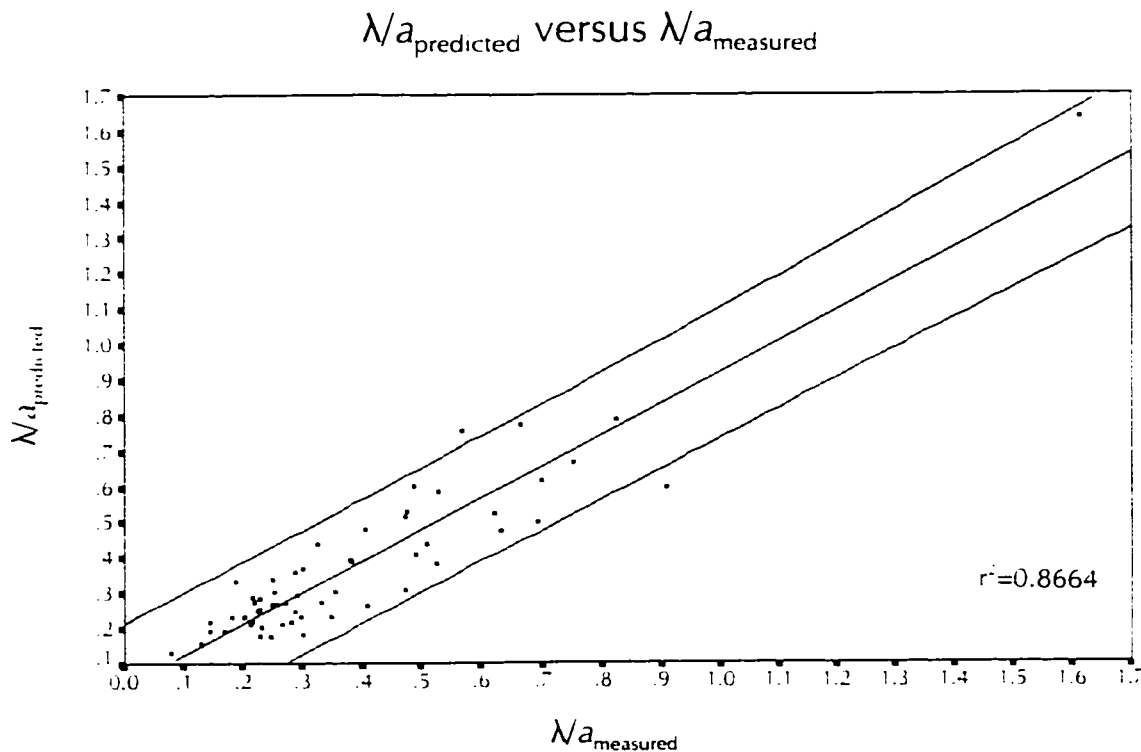


**Figure 20:** Predicted versus measured ripple wavelength for the primary data set (data shown in table 1) using the methods described in equation 7.

## 7.2 Assessment of Hypothesis #2

The second hypothesis attempted to determine if a relationship exists between ripple wavelength and the wave parameters as a function grain diameter. In order to evaluate this hypothesis it is necessary to determine if any relationship exists between  $\lambda/a$  and the mobility number ( $\psi$ ). Furthermore, it was conducive of this investigation to test Nielsen's (1981) predictive relationship (6), and to compare it to the predictive relationship (7).

Brebner (1980), Nielsen (1981), Clifton and Dingler (1984), and Wiberg and Harris (1994) relate ripple spacing to the "mobility number" ( $\psi$ ), (equation 2). According to Brebner (1980), as long as  $\psi$  is less than about 20 then the ripple length is proportional to the water semi-excursion ( $a$ ). Nielsen (1981) proposes that the spacing of naturally occurring ripples, in quartz sand (grain size of 210  $\mu\text{m}$ ), is best predicted by equation (6). However, as the mobility number increases, the ratio between  $\lambda/a$  begins to decrease until the ripples are wiped out completely. The results of this investigation make it possible to evaluate these conclusions, and determine if the semi-empirical formulae apply to a sand/mud environment.

When  $\lambda/a$  is plotted against  $\psi$  for all available field measurements, a strong inverse correlation is present with  $r^2=0.7049$  and  $r=-0.8396$  (Fig.21) (refer to Appendix II for statistical results). Therefore a sand/mud environment can have a mobility number in excess of 20 000 and not restrict ripple formation. Regression analysis of the data shown in Fig. 21, shows that natural ripple length in a sand/mud environment

is best predicted by:

$$\lambda/a = 13.12\psi^{-0.475} \quad (8)$$

Nielsen's (1981) predictive equation (6) shows a strong positive correlation between  $\lambda/a_{\text{predicted}}$  against  $\lambda/a_{\text{measured}}$ , with  $r^2=0.6879$  and  $r=0.829$  (Fig. 22) (refer to Appendix II for statistical results). However, equation (8) shows a much stronger positive correlation between  $\lambda/a_{\text{predicted}}$  against  $\lambda/a_{\text{measured}}$ , with  $r^2=0.7925$  and  $r=0.890$  (Fig. 23) (refer to Appendix II for statistical results).

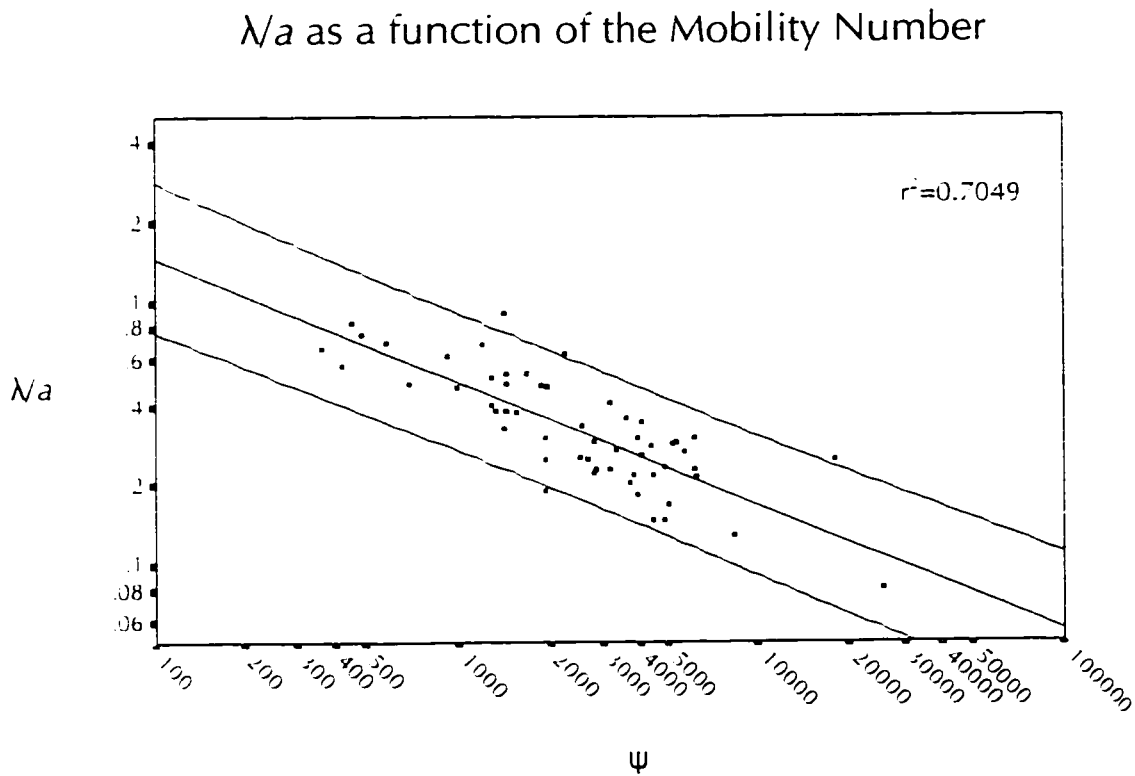


**Figure 21:** Measured ripple wavelength normalized by the water semi-excursion ( $\lambda/a$ ) as a function of the mobility number ( $\psi$ ).

$\lambda/a_{\text{predicted}}$  versus  $\lambda/a_{\text{measured}}$  (Nielsen, 1981)

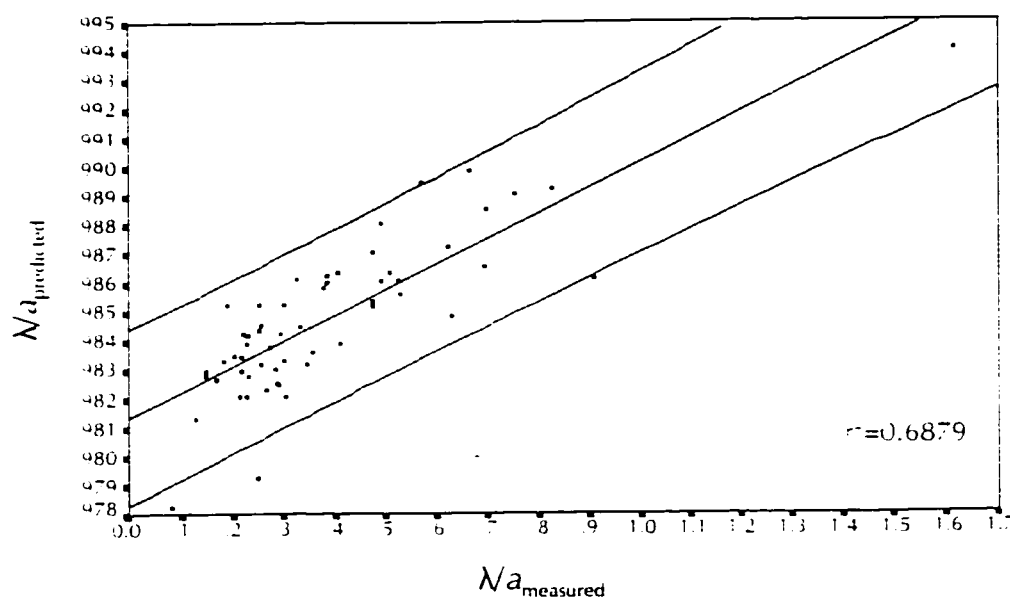


**Figure 22:** Predicted versus measured ripple wavelength ( $\lambda$ ) normalized by the water semi-excursion ( $a$ ) for the primary data set computed using the method of Nielsen (1981) (equation 6).

$\lambda/a_{\text{predicted}}$  versus  $\lambda/a_{\text{measured}}$

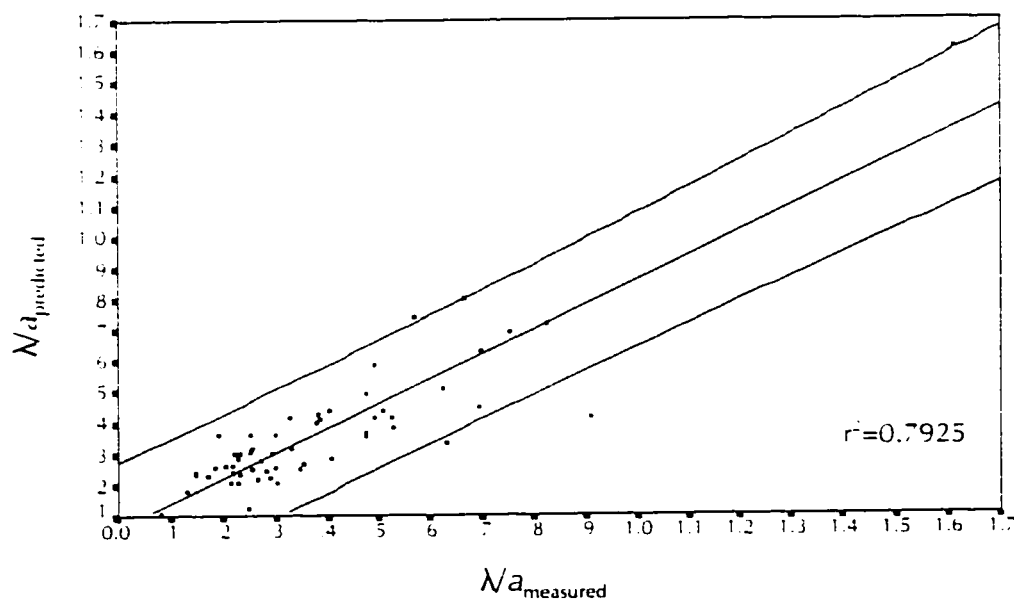


**Figure 23:** Predicted versus measured ripple wavelength ( $\lambda$ ) normalized by the water semi-excursion ( $a$ ) for the primary data set computed using the method described in this paper (equation 8).

Therefore, field observations suggest that by using  $d_o/D$  we may determine ripple type (orbital, suborbital, or anorbital), and compute ripple wavelength based on ripple type and flow characteristics. At  $d_o/D$  values ranging between 1054 and 14197 suborbital and anorbital ripples were successfully identified. Ripple spacing seemed to depend on orbital diameter and grain size for suborbital ripples, and only on grain size for anorbital ripples. Although ripple type is ambiguous, identifying which is more likely, under specific hydrodynamic conditions, would require further investigation possibly by comparing laboratory results with a similar sediment regime. As others have noted, orbital ripples dominate ripple types observed in laboratory studies, whereas anorbital ripples are the most commonly found type in field settings. This is a consequence of the fact that orbital ripples are generally found at smaller wave orbital diameters than are anorbital ripples. Given this, variations in ripple types are largely due to differences in wave period: the orbital diameter of oscillatory flows in wave tanks and tunnels being generally significantly lower than typically found in field settings. Thus the difference in ripple type in the two environments appears to be largely a result of the lack of substantial overlap in wave period in field and flume settings. Therefore, variations in wave period may further complicate the interpretive process in ways that are not yet fully understood.

This study provides a method for predicting ripple wavelength in a sand/mud environment that is simple and quite accurate. It avoids the distinctions between field and flume cases made by Nielsen (1981), and it provides better estimates for predicting anorbital ripple wavelength (equation 7). Unlike Brebner (1980), Nielsen



(1981), Clifton and Dingler (1984), and Wiberg and Harris (1994),  $\lambda/a$  shows a stronger correlation in this study with  $d_o/D$  than with the mobility number. This may be attributed to the finer sediments in the current investigation, although further investigation is need to confirm this assumption.

### 7.3 Suggestions for Further Study

Study of other areas is necessary in order to determine the general applicability of the author's findings. Sediment parameters and grain orientations of fossil sands should be studied. If similar methodologies produce results similar to the author's, their potential for interpreting paleo-environments is endless. Understanding wave-formed structures is best done in conjunction with geological evidence. Inferences of water depth or wave size based on wave-formed features are most credible when supported by other observations. For example, Allen (1981) used an approach similar to Nielsen (1981) to estimate the size and depth of a Devonian lake.

Future studies must make an attempt to incorporate ripple steepness (i.e., height) in order to develop a more accurate understanding of ripple formation and the factors that control their morphology. Possible suggestions include the *Ralph* sampling technique developed by Heffler (1984). *Ralph* samples all relevant hydrodynamic and ripple morphology data simultaneously, and records it electronically through a digital data logger. With such an instrument one may not only determine the variables which control ripple morphology but also determine migration rates, and changes in ripple morphology according to changes in

hydrodynamic conditions. Until specific and accurate data on ripple formation is made available, further comments on the factors affecting the morphology of ripple marks must remain largely speculative.

## CHAPTER 8.0

### CONCLUSIONS

The relationships between  $d_o/D$  and  $\lambda/D$ ;  $d_o/D$  and  $\lambda/a$ ; and  $\psi$  and  $\lambda/a$  have been examined for natural ocean waves in the nearshore zone in a sand/mud environment. Data have been collected from a range of wave energy conditions, and included grain sizes from 55.8-103.6  $\mu\text{m}$ . Data from the field and laboratory experiments of Inman (1957), Dingler (1974), Clifton (1976), Miler and Komar (1980a,b), Nielsen (1981), Clifton and Dingler (1984), and Wiberg and Harris (1994) were compared with data collected in this study off the coast Guyana, South America. Initially, the relationship between  $d_o/D$  and the resulting  $\lambda/D$  was analysed to determine ripple classification (orbital, suborbital, or anorbital). All field data were then compared with the relationship:

$$\lambda \approx 400D \sim 600D \quad (3)$$

for anorbital ripples, based upon data obtained in field setting by various investigators under complex oscillatory water motions. Ripple spacing ( $\lambda/a$ ) data as a function of orbital diameter  $d_o/D$  were compared with Nielsen's (1981) empirical relationship:

$$\lambda/a = \exp[(693 - 0.37 \ln^8 \psi) / (1000 + 0.75 \ln^7 \psi)] \quad (6)$$

The final analysis involved relating ripple spacing ( $\lambda/a$ ) to the mobility number ( $\psi$ ). A summary of the results are as follows:

- i. Four ripple types can be differentiated on the basis of wavelength, nature of the crest, orientation, and sinuosity: straight; sinuous; linguoid ripple; and catenary ripple-trains.

- ii. Ripple wavelength is a complicated function of the flow and sediment parameters. Although no relationship was identified by comparing  $\lambda/D$  with  $d_o/D$ , it was possible to successfully classify the ripple data. Forty percent of the ripples were classified as **suborbital**, while the remaining 60% were **anorbital**. These results are in accordance with the work of others, in that suborbital and anorbital ripples are most common in field settings, while orbital are most common in laboratory settings.
- iii. The work of others suggest that anorbital ripples, with a sediment regime  $>125 \mu\text{m}$  in diameter, follow relationship (3), however, this investigation suggests that in a sand/mud environment, the following relationship may be more appropriate:

$$\lambda = 514D - 1540D \quad (4)$$

- iv. Generally  $\lambda$  is of the same order of magnitude as the water semi-excursion ( $a$ ). A strong inverse relationship between  $\lambda/a$  and the mobility number was observed with  $r^2=0.7049$ . Using Nielsen's (1981) predictive relationship (6) for field settings showed a fair positive correlation between  $\lambda/a_{\text{predicted}}$  and  $\lambda/a_{\text{measured}}$  with  $r^2=0.6879$ . However, in the sand/mud environment of Guyana, a stronger correlation was observed ( $r^2=0.7925$ ) employing the following equation:

$$\lambda/a = 13.12\psi^{-0.475} \quad (8)$$

- v. The single most important parameter determining  $\lambda/a$  in a sand/mud environment was found to be  $d_o/D$ . When  $\lambda/a$  was plotted against  $d_o/D$  the data showed a strong inverse relationship with  $r^2=0.7936$ . Thus ripple wavelength are completely specified given  $a$ , and mean grain size ( $D$ ). The following equation was found to best predict  $\lambda/a$  in a sand/mud environment:

$$\lambda/a = 1419.06 d_r/D^{-0.972} \quad (7)$$

Correlating  $\lambda/a_{\text{predicted}}$  against  $\lambda/a_{\text{measured}}$  provided an  $r^2$  value of 0.8664.

The concepts and calculations described here can be applied to the interpretation of wave-formed ripples in shallow marine environments. However, further field and laboratory work must be undertaken before we can fully understand the factors that affect ripple morphology, and use this information to confidently reconstruct paleoenvironmental conditions. At present, we can only provide powerful, but often tantalizing, clues regarding the potential truth behind ripple morphology.

## REFERENCES

- Allen, J. R. L. 1968. Current Ripples. Amsterdam: North-Holland Publishing Company.
- Allen, J. R. L. 1979. A model for the interpretation of wave ripple-marks using their wavelength, textural composition, and shape. J. of the Geo. Soc. of London, 136: pp. 673-82.
- Allen, J. R. L. 1982. Sediment structures: their character and physical basis. Developments in Sedimentology, 30A, Vol. 1. Elsevier, Amsterdam, pp. 593.
- Allen, P. A. 1981. Some guidelines in reconstructing ancient sea conditions from wave ripples. Marine Geology, 43: pp. M59-M67
- Allersma, E. 1968. Mud on the oceanic shelf off Guiana. Paper presented at Cicar Symposium, Curacao.
- Aspler, L. B., Chiarenzelli, J. R., and Bursey, T. L. 1994. Ripple marks in quartz arenites of the Hurwitz group, Northwest Territories, Canada: Evidence for sedimentation in a vast, early Proterozoic, Shallow. Fresh-water lake. J. of Sed. Res., vol. A64, No. 2, pp. 282-298.
- Baas, J. H. 1994. A flume study on the development and equilibrium morphology of current ripples in very fine sand. Sedimentology, 41: pp. 185-209.
- Baas, J. H., and De Koning, H. 1995. Washed-out ripples: their equilibrium dimensions, migration rate, and relation to suspended-sediment concentration in very fine sand. J. of Sed. Res., Vol. A65, No. 2, pp. 431-435.
- Bagnold, R. A. 1946. Motion of waves in shallow water-interaction between waves and sand bottoms. Proc. Royal Society of London, 187A: pp. 1-15.
- Berbrner, A. 1980. Sand bed-form lengths under oscillatory flow. Proc. 17th Coastal Engrn. Conf., pp. 1341-3.
- Boyd, R., Forbes, D. L., and Heffler, D. E. 1988. Time-sequence observations of wave-formed sand ripples on an ocean shoreface. Sedimentology, 35: pp. 449-64.
- Brinkman Instruments Inc. 1988. PSA 2010 Particle Size Analyzer: Operation Manual.
- Carstens, M. R., Neilson, F. M., and Altinbilek, H. D. 1969. Bed forms generated in the laboratory under an oscillatory flow. Tech. Memo No. 28, U.S. Corps of Engrn., Coastal Engrn. Res. Cent., Washington, D.C..
- Clifton, H. E. 1976. Wave-formed sedimentary structures: A conceptual model. In: Beach and Nearshore Sedimentation, eds. R. A. Davis and R. L. Ethington. Society of Economic Paleontologists and Mineralogists, Oklahoma, U.S.A., No. 24

- Clifton, H. E. and Dingler, J. R. 1984. Wave-formed structures and paleo-environmental reconstruction. Marine Geology, 60: pp. 165-98.
- Cornish, V. 1934. Ocean Waves. CUP, Cambridge.
- Chorley, R. J., and Kennedy, R. W. 1971. Introduction. In: Water, Earth and Man, ed. R. J. Chorley. London, Methuen: pp. 1-7
- Darwin, G. H. 1884. Proc. Roy. Soc. London, 36: 18-43.
- Dingler, J. R., Boylls, J. C., and Lowe, R. L. 1977. A high frequency sonar for profiling small-scale subaqueous bedforms. Marine Geology, 24, pp. 279-288.
- Dingler, J. R. and Inman, D. L. 1976. Wave-formed ripples in nearshore sands. Proc. 15th Coastal Engnr. Conf., pp. 2109-21.
- Dyer, K. R. 1986. Coastal and Estuarine Sediment Dynamics, Wiley, Chichester, U.K.
- Froidefond, J. M., Pujos, M., Andre, X. 1988. Migration of mud banks and changing coastline in French Guiana. Marine Geology, 84: pp. 19-30.
- Grant, W. D., and Madsen O. S. 1982. Movable Bed Roughness in Unsteady Oscillatory Flow. J. Geophys. Res., 87, pp. 469-481.
- Heifler, D. E. 1984. RALPH-an instrument to monitor seabed sediments. Pap. Geol. Surv. Canada, 84-1B, pp. 47-52.
- Horikawa, K., and Watanabe, A. 1967. A study on sand movement due to wave action. Coastal Engnr. Japan, 10: pp. 469-481.
- Inman, D. L. 1957. Wave-generated ripples in nearshore sands. Tech. Memo No. 100, U.S. Corps of Engnr., Beach Erosion Board., Washington D.C..
- Johnston, R. J. 1980. Multivariate Statistical Analysis in Geography. John Wiley & Sons Inc., New York.
- Kawata, Y., Shirai, T., and Tsuchiya, Y. 1992. Field observation on sand ripples under rough sea state. Proc. 23rd Coastal Engnr. Conf., pp. 2164-75.
- Kennedy, J.F. and Falcon, M. 1965. Wave generated sediment ripples. Rep. 86, Mass. Inst. of Technol. Hydrodyn. Lab., Cambridge.
- Komar, P. D. 1974. Oscillatory ripple marks and the elevation of ancient wave conditions and environments. J. of Sediment Petrol., 44: pp. 169-180.
- Kos'yan, R. D. and Kochergin, A. D. 1992. About conditions for the wave ripple existence. Proc. 23rd Coastal Engnr. Conf., pp. 2176-90.

- Lakhan, V. C., 1994. Planning and development in the coastal zone of Guyana. Ocean & Coastal Management, 22, pp. 169-186.
- Loiquist, K. E. B. 1978. Sand ripples growth in an oscillatory-flow water tunnel. Tech. Paper, Coastal Eng. Res. Center, Washington, D.C., pp. 78-5.
- Manohar, M. 1955. Mechanisms of bottom sediment movement due to wave action. Technical Memo No. 75, U.S. Corps of Engr., Beach Erosion Board, Washington, D.C..
- Marsh-McBirney Inc. 1990. MMI Model 2000 Flo-Mate Portable Water Flowmeter Instruction Manual, Maryland.
- Miller, M. C. and Komar, P. D. 1980a. Oscillation sand ripples generated by laboratory apparatus. J. of Sediment Petrol., 50: pp. 173-82.
- Miller, M. C. and Komar, P. D. 1980b. A field investigation of the relationship between oscillation ripple spacing and the near-bottom water orbital motions. J. of Sediment Petrol., 50: pp. 183-91.
- Mogridge, G. R., Davies, M. H., and Willis, D. H. 1994. Geometry prediction for wave-generated bedforms. Coastal Engnr., 22: pp. 255-86.
- Mogridge, G. R. and Kamphuis, J. W. 1972. Experiments on bed form generation by wave action. Proc. 13th Coastal Engnr. Conf., pp. 1123-42.
- Newton, R. S. 1968. Internal structures of wave-formed ripple marks in the nearshore zone. Sedimentology, 11, pp. 275-292.
- Nielsen, P. 1981. Dynamics and geometry of wave-generated ripples. J. Geophys. Res., 86: pp. 6467-72.
- Nota, D. J. G. 1958. Sediments of the western guiana shelf. H. Veenman & Zonen, Wageningen, pp. 103.
- Oost, A. P., and Baas, J. H. 1994. The development of small scale bedforms in tidal environments: an empirical model for unsteady flow and its application. Sedimentology, 41, pp. 883-903.
- Osborne, P. D. and Vincent, C. E. 1993. Dynamics of large and small scale bedforms on a macrotidal shoreface under shoaling and breaking waves, Marine Geology., 115: pp. 207-26.
- Ranasoma, K. I. M. and Sleath, J. F. A. 1992. Velocity measurements close to rippled beds. Proc. 23rd Coastal Engnr. Conf., pp. 2383-96.
- Sleath, J. F. A. 1975. A contribution to the study of vortex ripples. J. of Hydraulic Res., 13: pp. 315-28.



- Trenhaile, A. S. 1973. Near-shore ripples: some hydraulic relationships. J. of Sediment Petrol., 43: pp. 558-68.
- Trenhaile, A. S. In press. Coastal Dynamics and Landforms, Oxford University Press, Oxford, UK.
- Vongvisessomjai, S. 1984. Oscillatory ripple geometry. J. of Hydraulic Eng., 110: pp. 247-66.
- Wiberg, P. L. and Harris, C. K. 1994. Ripple geometry in wave-dominated environments. J. Geophys. Res., 99: pp. 775-89.
- Yalin, M. S. and Russell, R. C. H. 1962. Similarity in sediment transport due to waves. Proc. 8th Coastal Engr. Confr., pp. 151-167.

## **APPENDIX I**

### Glossary

Brinkpoint is the point on a ripple that separates the slipface from the crestal shoulder.

Crestal platform is a flat, almost level area on the crest of a ripple situated between the platform line and the crestline.

Catenary describes a ripple whose span is many times the wavelength and whose crestline in plan is divided up into a series.

Crest is that part of a ripple which is in elevation above the troughline exceeds half of the ripple height.

Height is the vertical distance between troughline and the crestline.

Leeside refers to the steeply sloping part of a ripple extending downstream from the crestline as far as the troughline.

Linguoid describes a ripple whose span is considerable to the wavelength and whose crest is strongly curved.

Lunate describes a ripple whose crest is strongly curved.

Phase describes the relationship between ripples in a train. Ripples are said to be *in phase* when they, or the elements of their crests, are arranged in rows parallel to flow. Ripples are said to be *out of phase* when they, or the arbitrary elements of their crests, are arranged in rows diagonal to flow.

Platformpoint is that point on a vertical profile through a ripple that lies at the upstream edge of the crestal platform.

Sinuuous describes a ripple whose span is many times the chord and whose crestline swings smoothly from side to side as viewed from above.

Slipface is a steeply sloping portion of the leeside of a ripple, lying between the brinkpoint and the troughpoint.

Smallscale ripples are less than 60 cm in wavelength and smaller than 4 cm in height.

Span is the horizontal distance, measured at right angles to flow, between the extremities of a ripple.

Stoss-side is the gently sloping, eroded side of a ripple between the brinkpoint and the troughpoint.

Straight ripples have a span many times the chord and whose crestline is essentially rectilinear in plan.

Summitpoint is the point of maximum elevation on the vertical profile of a ripple. Divides the stoss-side from the leeside.

Swept describes a long-crested ripple whose crestline differs substantially from those at right angles to flow.

Transverse describes a long-crested ripple whose crestline is substantially at right angles to flow as determined by independent means.

Trough is that part of a ripple where the elevation above the troughline is less than half the ripple height.

Troughpoint is that point of minimum elevation on the vertical profile of a ripple. Divides the leeside from the stoss-side.

Wavelength is the horizontal distance, parallel to flow, between the troughline or crestline of one ripple to the troughline or crestline of the next ripple down flow.

## **APPENDIX II**

### Statistical Reports

**Multiple regression corresponding to the results in figure 17**

	Mean	Std Dev	Label
log $\Lambda/D$	2.956	.107	
log do/D	3.736	.216	

N of Cases =58

Correlation, 1-tailed Sig:

	log $\Lambda/D$	log do/D
log $\Lambda/D$	1.000	.056 .337
log do/D	.056 .337	1.000 .

Equation Number 1      Dependent Variable..      log  $\Lambda/D$

Block Number 1.    Method: Stepwise      Criteria    PIN   .0500  
POUT   .1000  
log do/D

End Block Number    1    PIN =      .050 Limits reached.  
No variables entered/removed for this block.

**Multiple regression corresponding to the results in figure 18.**

	Mean	Std Dev	Label
log $\Lambda/a$	-.479	.235	
log do/D	3.736	.216	

N of Cases =58

Correlation, 1-tailed Sig:

	LOGRW_A	LOGDO_D
log $\Lambda/a$	1.000	-.891 .000
log do/D	-.891 .000	1.000 .

Equation Number 1      Dependent Variable..      LOGRW\_A

Block Number 1.    Method:    Stepwise      Criteria    PIN    .0500  
 POUT    .1000  
 log do/D

Step	MultiR	Rsq	F(Eqn)	SigF	Variable	BetaIn
1	.8909	.7936	215.358	.000	In: LOGDO_D	-.8909

Variables Entered on Step Number  
 1..      log do/D

Multiple R	-.89086
R Square	.79363
Adjusted R Square	.78995
Standard Error	.10783

#### Analysis of Variance

	DF	Sum of Squares	Mean Square
Regression	1	2.50418	2.50418
Residual	56	.65117	.01163

F =215.35810      Signif F =.0000

Var-Covar Matrix of Regression Coefficients (B)  
 Below Diagonal: Covariance      Above: Correlation

	log do/D
log do/D	.00439

Equation Number 1      Dependent Variable..      log A/D

----- Variables in the Equation -----

Variable	B	SE B	95% Confdnce	Intrvl B	Beta
log do/D	-.971980	.066233	-1.104661	-.839298	-.890859
(Constant)	3.152029	.247865	2.655495	3.648563	

----- Variables in the Equation -----

Variable	Tolerance	VIF	T	Sig T
log do/D	1.000000	1.000	-14.675	.0000
(Constant)			12.717	.0000

#### Collinearity Diagnostics

Number	Eigenval	Cond	Variance Proportions
--------	----------	------	----------------------

		Index	Constant	log dc/D
1	1.99837	1.000	.00082	.00082
2	.00163	34.983	.99918	.99918

End Block Number 1 POUT = .100 Limits reached.

Equation Number 1 Dependent Variable.. log A/a

Residuals Statistics:

	Min	Max	Mean	Std Dev	N
*PRED	-.8838	.2136	-.4795	.2096	58
*ZPRED	-1.9291	3.3067	.0000	1.0000	58
*SEPPRED	.0142	.0493	.0192	.0059	58
*ADJPRED	-.3649	.2152	-.4793	.2095	58
*RESID	-.2447	.2241	.0000	.1069	58
*ZRESID	-2.2695	2.0787	.0000	.9912	58
*SRESID	-2.2893	2.1270	-.0007	1.0084	58
*DRESID	-.2490	.2347	-.0002	.1106	58
*SDRESID	-2.3830	2.1986	.0000	1.0217	58
*MAHAL	.0003	10.9341	.9828	1.5954	58
*COOK D	.0000	.1866	.0177	.0295	58
*LEVER	.0000	.1918	.0172	.0280	58

Total Cases = 58

Durbin-Watson Test = 1.39246

---

Multiple regression corresponding to the results in figure 20.

	Mean	Std Dev	Label
A/a(pred)	.377	.234	
A/a(meas)	.386	.247	

N of Cases =58

Correlation, 1-tailed Sig:

	A/a(pred)	A/a(meas)
A/a(pred)	1.000	.931
	.	.000
A/a(meas)	.931	1.000
	.000	.

Equation Number 1 Dependent Variable.. A/a(pred)



Block Number 1. Method: Stepwise Criteria PIN .0500  
 POUT .1000  
 $\Delta/a(\text{meas})$

Step	MultR	Rsq	F(Eqn)	SigF	Variable	BetaIn
1	.9308	.8664	363.220	.000	In: $\Delta/a(\text{meas})$	.9308

Variable(s) Entered on Step Number  
 1..  $\Delta/a(\text{meas})$

Multiple R .93082  
 R Square .86642  
 Adjusted R Square .86403  
 Standard Error .08645

Analysis of Variance			
	DF	Sum of Squares	Mean Square
Regression	1	2.71428	2.71428
Residual	56	.41848	.00747

F = 363.22034 Signif F = .0000

Var-Covar Matrix of Regression Coefficients (B)  
 Below Diagonal: Covariance Above: Correlation

$\Delta/a(\text{meas})$

$\Delta/a(\text{meas})$  .00214

Equation Number 1 Dependent Variable..  $\Delta/a(\text{pred})$

----- Variables in the Equation -----					
Variable	B	SE B	95% Confidence	Intrvl B	Beta
$\Delta/a(\text{meas})$	.382604	.046311	.789832	.975375	.930816
(Constant)	.036299	.021177	-.006124	.078723	

----- Variables in the Equation -----				
Variable	Tolerance	VIF	T	Sig T
$\Delta/a(\text{meas})$	1.000000	1.000	19.058	.0000
(Constant)			1.714	.0920

Collinearity Diagnostics

Number	Eigenval	Cond Index	Variance Proportions	
			Constant	$\Delta/a(\text{meas})$
1	1.84422	1.000	.07789	.07789
2	.15578	3.441	.92211	.92211

End Block Number 1 POUT = .100 Limits reached.

Equation Number 1      Dependent Variable..       $\Lambda/a(\text{pred})$

Residuals Statistics:

	Min	Max	Mean	Std Dev	N
*PRED	.1073	1.4602	.3770	.2182	58
*ZPRED	-1.2358	4.9635	.0000	1.0000	58
*SEPPRED	.0114	.0580	.0147	.0065	58
*ADJPPRED	.1063	1.3174	.3750	.2076	58
*RESID	-.2404	.2147	.0000	.0857	58
*ZRESID	-2.7813	2.4837	.0000	.9912	58
*SRESID	-2.9245	2.7260	.0099	1.0372	58
*DRESID	-.2658	.3176	.0021	.0954	58
*SDRESID	-3.1486	2.9009	.0104	1.0673	58
*MAHAL	.0001	24.6367	.9828	3.2551	58
*COOK D	.0000	3.0334	.0705	.4005	58
*LEVER	.0000	.4322	.0172	.0571	58

Total Cases =            58

Durbin-Watson Test =    1.31896

---

Multiple regression corresponding to the results in figure 21.

	Mean	Std Dev	Label
log $\Lambda/a$	-.479	.235	
log $\Psi$	3.366	.416	

N of Cases = 58

Correlation, 1-tailed Sig:

	log $\Lambda/a$	log $\Psi$
log $\Lambda/a$	1.000	-.840
	.	.000
log $\Psi$	-.840	1.000
	.000	.

Equation Number 1      Dependent Variable..      log  $\Lambda/a$

Block Number 1.    Method:    Stepwise      Criteria    PIN    .0500  
 POUT    .1000  
 log  $\Psi$

Step	MultR	Rsqr	F(Eqn)	SigF	Variable	BetaIn
------	-------	------	--------	------	----------	--------

1 .8396 .7049 133.777 .000 In:log  $\psi$  -.8396

Variable(s) Entered on Step Number

1.. log  $\psi$

Multiple R -.83959  
R Square .70492  
Adjusted R Square .69965  
Standard Error .12894

Analysis of Variance

	DF	Sum of Squares	Mean Square
Regression	1	2.22426	2.22426
Residual	56	.93109	.01663

F = 133.77697 Signif F = .0000

Var-Covar Matrix of Regression Coefficients (B)

Below Diagonal: Covariance Above: Correlation

log  $\psi$

log  $\psi$  .00168

Equation Number 1 Dependent Variable.. Log A/a

----- Variables in the Equation -----

Variable	B	SE B	95% Confidence	Intervl B	Beta
log $\psi$	-.474616	.041035	-.556818	-.392413	-.839593
(Constant)	1.118159	.139163	.839381	1.396936	

----- Variables in the Equation -----

Variable	Tolerance	VIF	T	Sig T
Log $\psi$	1.000000	1.000	-11.566	.0000
(Constant)			8.035	.0000

Collinearity Diagnostics

Number	Eigenval	Cond Index	Variance Proportions Constant	Variance Proportions Log $\psi$
1	1.99257	1.000	.00371	.00371
2	.00743	16.378	.99629	.99629

End Block Number 1 POUT = .100 Limits reached.

Equation Number 1 Dependent Variable.. log A/a

Residuals Statistics:

	Min	Max	Mean	Std Dev	N
*PRED	-.9743	.2072	-.4795	.1975	58
*ZPRED	-2.5049	3.4759	.0000	1.0000	58
*SEPPRED	.0169	.0617	.0225	.0081	58
*ADJPRED	-.9568	.2070	-.4795	.1981	58
*RESID	-.2794	.3353	.0000	.1278	58
*ZRESID	-2.1666	2.6000	.0000	.9912	58
*SRESID	-2.1863	2.6290	.0003	1.0083	58
*DRESID	-.2845	.3428	.0001	.1323	58
*SDRESID	-2.2655	2.7828	.0040	1.0277	58
*MAHAL	.0013	12.0819	.9828	1.9172	58
*COOK D	.0000	.3080	.0178	.0421	58
*LEVER	.0000	.2120	.0172	.0336	58

Total Cases = 58

Durbin-Watson Test = .74572

---

Multiple regression corresponding to the results in figure 22.

	Mean	Std Dev	Label
$\Delta/a(\text{pred})$	.985	.003	
$\Delta/a(\text{meas})$	.386	.247	

N of Cases = 58

Correlation, 1-tailed Sig:

	$\Delta/a(\text{pred})$	$\Delta/a(\text{meas})$
$\Delta/a(\text{pred})$	1.000	.829
	.	.000
$\Delta/a(\text{meas})$	.829	1.000
	.000	.

Equation Number 1      Dependent Variable..       $\Delta/a(\text{pred})$

Block Number 1.    Method: Stepwise      Criteria    PIN    .0500  
 POUT    .1000  
 $\Delta/a(\text{meas})$

Step	MultR	Rsq	F(Eqn)	SigF	Variable	BetaIn
1	.8294	.6879	123.407	.000	In: $\Delta/a(\text{meas})$	.8294

Variable(s) Entered on Step Number  
 1..  $\Delta/a(\text{meas})$

Multiple R .82937  
 R Square .68786  
 Adjusted R Square .68229  
 Standard Error 1.47779E-03

Analysis of Variance			
	DF	Sum of Squares	Mean Square
Regression	1	.00027	.00027
Residual	56	.00012	.00000

F = 123.40740 Signif F = .0000

Var-Covar Matrix of Regression Coefficients (B)  
 Below Diagonal: Covariance Above: Correlation

$\Delta/a(\text{meas})$

$\Delta/a(\text{meas})$  6.268E-07

Equation Number 1 Dependent Variable..  $\Delta/a(\text{pred})$

----- Variables in the Equation -----

Variable	B	SE B	95% Confidence Interval B	Beta
$\Delta/a(\text{meas})$	.008795	7.9168E-04	.007209 .010381	.829374
(Constant)	.981352	3.6203E-04	.980627 .982077	

----- Variables in the Equation -----

Variable	Tolerance	VIF	T	Sig T
$\Delta/a(\text{meas})$	1.000000	1.000	11.109	.0000
(Constant)			2710.727	.0000

Collinearity Diagnostics

Number	Eigenval	Cond Index	Variance Proportions	
			Constant	$\Delta/a(\text{meas})$
1	1.84422	1.000	.07789	.07789
2	.15578	3.441	.92211	.92211

End Block Number 1 POUT = .100 Limits reached.

Equation Number 1      Dependent Variable..       $\Delta/a(\text{pred})$

Residuals Statistics:

	Min	Max	Mean	Std Dev	N
*PRED	.9821	.9955	.9847	.0022	58
*ZPRED	-1.2358	4.9635	.0000	1.0000	58
*SEPRE	.0002	.0010	.0003	.0001	58
*ADJPRED	.9822	.9968	.9848	.0023	58
*RESID	-.0043	.0031	.0000	.0015	58
*ERESID	-2.8996	2.0754	.0000	.9912	58
*SRESID	-2.9332	2.1040	-.0075	1.0159	58
*DRESID	-.0044	.0032	.0000	.0015	58
*SDRESID	-3.1597	2.1728	-.0136	1.0435	58
*MAHAL	.0001	24.6367	.9828	3.2551	58
*COOK D	.0000	.7998	.0314	.1117	58
*LEVER	.0000	.4322	.0172	.0571	58

Total Cases =            58

Durbin-Watson Test =    1.11416

---

Multiple regression corresponding to the results in figure 23.

	Mean	Std Dev	Label
$\Delta/a(\text{pred})$	.371	.222	
$\Delta/a(\text{meas})$	.386	.247	

N of Cases = 58

Correlation, 1-tailed Sig:

	$\Delta/a(\text{pred})$	$\Delta/a(\text{meas})$
$\Delta/a(\text{pred})$	1.000	.890
	.	.000
$\Delta/a(\text{meas})$	.890	1.000
	.000	.

Equation Number 1      Dependent Variable..       $\Delta/a(\text{pred})$

Block Number 1.    Method:    Stepwise      Criteria    PIN    .0500  
 POUT    .1000  
 $\Delta/a(\text{meas})$

Step	MultR	Rsq	F(Eqn)	SigF	Variable	BetaIn
1	.8902	.7925	213.826	.000	In: $\Delta/a(\text{meas})$	.8902

Variable(s) Entered on Step Number  
 1.. A/a(meas)

Multiple R .89020  
 R Square .79246  
 Adjusted R Square .78875  
 Standard Error .10225

Analysis of Variance

	DF	Sum of Squares	Mean Square
Regression	1	2.23535	2.23535
Residual	56	.58543	.01045

F = 213.82563 Signif F = .0000

Var-Covar Matrix of Regression Coefficients (B)  
 Below Diagonal: Covariance Above: Correlation

A/a(meas)

A/a(meas) .00300

Equation Number 1 Dependent Variable.. A/a(pred)

----- Variables in the Equation -----

Variable	B	SE B	95% Confidence Interval B	Beta
A/a(meas)	.800961	.054775	.691233 .910688	.890201
(Constant)	.061343	.025048	.011166 .111520	

----- Variables in the Equation -----

Variable	Tolerance	VIF	T	Sig T
A/a(meas)	1.000000	1.000	14.623	.0000
(Constant)			2.449	.0175

Collinearity Diagnostics

Number	Eigenval	Cond Index	Variance Proportions Constant	A/a(meas)
1	1.84422	1.000	.07789	.07789
2	.15578	3.441	.92211	.92211

End Block Number 1 POUT = .100 Limits reached.

Equation Number 1 Dependent Variable.. A/a(pred)

# Residuals Statistics:

	Min	Max	Mean	Std Dev	N
*PRED	.1258	1.3535	.3706	.1980	58
*ZPRED	-1.2358	4.9635	.0000	1.0000	58
*SEPRE	.0134	.0685	.0174	.0077	58
*ADJPRED	.1268	1.1460	.3676	.1831	58
*RESID	-.3705	.2542	.0000	.1013	58
*ZRESID	-3.6236	2.4858	.0000	.9912	58
*SRESID	-3.8101	3.3502	.0121	1.0554	58
*DRESID	-.4096	.4617	.0030	.1175	58
*SDRESID	-4.3872	3.7130	.0089	1.1237	58
*MAHAL	.0001	24.6367	.9828	3.2551	58
*COOK D	.0000	4.5816	.1017	.6071	58
*LEVER	.0000	.4322	.0172	.0571	58

Total Cases = 58

Durbin-Watson Test = .86633

## Index of Residual Statistics

Name	Contents
----	-----
*PRED	Unstandardized predicted values
*ZPRED	Standardized predicted values
*SEPRE	Standard error of mean predictions
*ADJPRED	Adjusted predicted values
*RESID	Unstandardized residuals
*ZRESID	Standardized residuals
*SRESID	Studentized residuals
*DRESID	Deleted residuals
*SDRESID	Studentized deleted residuals
*MAHAL	Mahalanobis Distances
*COOK D	Cook's Distances
*LEVER	Leverage Distance Values



## **VITA AUCTORIS**

NAME: Josip Curkovic Jr.

PLACE OF BIRTH: Ottawa, Ontario, CA

YEAR OF BIRTH: 1966

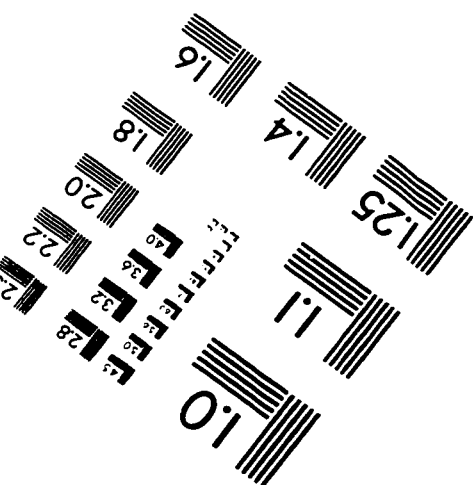
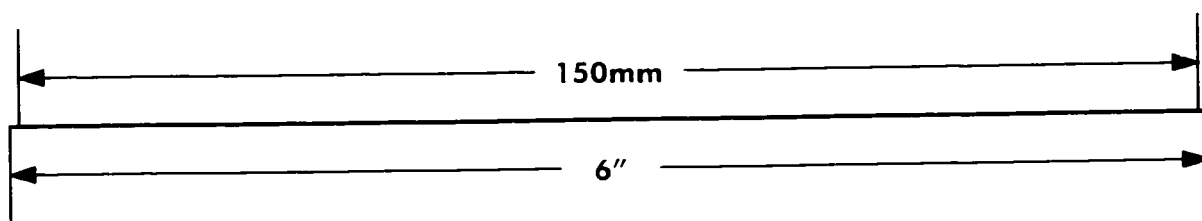
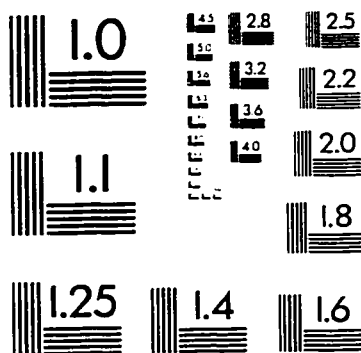
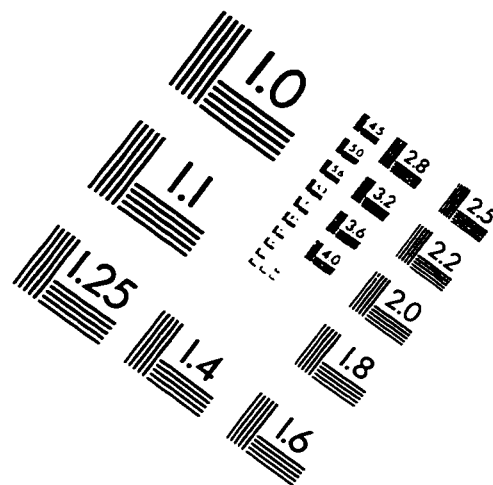
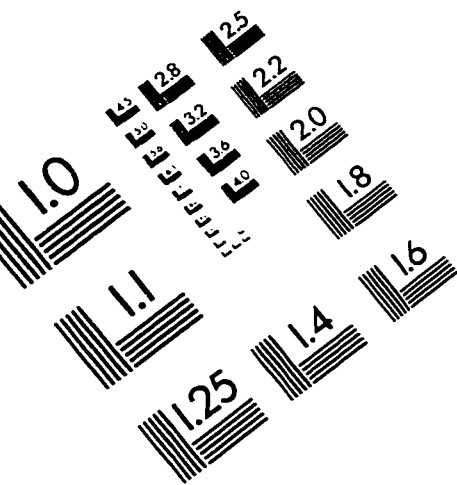
EDUCATION: Sir Robert Borden High School, Ottawa, Ontario  
1983-1987

University of Windsor, Windsor, Ontario  
1988-1993 B.A. Geography (Env. Resource Management)

University of Windsor, Windsor, Ontario  
1993-1996 M.A. Geography

University of Western Ontario, London, Ontario  
1995-1996 B.Ed

# IMAGE EVALUATION TEST TARGET (QA-3)



APPLIED IMAGE, Inc  
1653 East Main Street  
Rochester, NY 14609 USA  
Phone: 716/482-0300  
Fax: 716/288-5989

© 1993, Applied Image, Inc., All Rights Reserved

